Universidade Federal do Rio Grande do Sul
Programa de Pós-Graduação em Física

Dissertação de Mestrado

Interaction between metal surfaces inside an electrolyte solution

(Interação entre superfícies metálicas no interior de uma solução eletrolítica[1])

Rodrigo Mór Malossi

Trabalho sob a orientação do professor Yan Levin.

Porto Alegre
Março, 2019

[1]Trabalho parcialmente financiado pelo Conselho Nacional de Desenvolvimento Científico e Tecnológico (CNPq).

Abstract

In this Dissertation, we present a new method to study metal surfaces inside an electrolyte solution. In order to do that, we start with a review of an efficient 3D Ewald Summation technique which considers the plate fields as external potentials. Then we present a solution to the Poisson Equation for confined systems that uses periodic Green functions, which allow us to avoid minimization procedures to compute the induced charges at the boundaries. This formalism is applied to a lattice model of an ionic liquid to capture the characteristic capacitance shape transition of the system. Finally, we develop the new method by extending those techniques to include an electrolyte in the outer regions of the plates. A preliminary test of the method is done by obtaining density profiles for a system of neutral plates inside electrolyte solutions with monovalent and trivalent ions.

Resumo

Nesta Dissertação nós apresentamos um método novo para o estudo de superfícies metálicas no interior de uma solução eletrolítica. Para isso, começamos com uma revisão de uma técnica eficiente para somas de Ewald 3D que considera os campos das placas como potenciais externos. Então nós mostramos uma solução para a Equação de Poisson para sistemas confinados que utiliza funções de Green periódicas, a qual nos permite evitar a utilização de procedimentos de minimização para computar as cargas induzidas nos contornos. Esse formalismo é aplicado para um modelo de rede de um líquido iônico para capturar a transição característica de forma da capacitância do sistema. Finalmente, nós desenvolvemos o novo método estendendo essas técnicas para incluir um eletrólito nas regiões externas das placas. Um teste preliminar do método é feito pela obtenção de perfis de densidade para um sistema de placas neutras no interior de uma solução eletrolítica com íons monovalentes e trivalentes.

Acknowledgments

- To the Institute of Physics (UFRGS) for the opportunity and the resources.
- To Yan Levin for the dedicated supervision and guidance.
- To Matheus Girotto and Alexandre dos Santos for the many insightful discussions.
- To my family for all the encouragement, patience, and support.

Published Papers

- Girotto, M.; **Malossi, R. M.**; dos Santos; A. P., Levin, Y; Lattice model of ionic liquid confined by metal electrodes *J. Chem. Phys.* **2018**, *148*, 193829

Contents

1 Introduction

Simulations play a fundamental role in all fields of science today. However, several of the current techniques are still based on ideas that were invented together with the development of the first computers [1].

In physics, the Monte Carlo method has had an interesting history. Back in 1949 Metropolis and Ulam presented a review of the use of the method in simulations with 'modern computing machines' [2]. Together with Fermi and von Neumann they began considering the use of random numbers to examine different problems in physics from this new stochastic perspective [3]. In the classic, Metropolis method [4] a transition probability is used to generate configurations from a previous state. The probability depends on the energy difference between the initial and final states. This very earliest work laid the foundations of modern Monte Carlo simulation [5].

The technique employed in this study is still widely used and it was developed to simulate in two dimensions (the original models were highly idealized representations of molecules, such as hard spheres and disks), and it was tested with theoretical predictions using virial expansions [4]. Within a few years, Monte Carlo simulations were carried out on the Lennard-Jones interaction potential [6]. This made it possible to compare data obtained from experiments on, for example, liquid argon, with the computer-generated thermodynamic data derived from a model [5]. The algorithm is revolutionary, it is used in several fields of physics, and it is still at the basis of our new method.

In the present work, we are concerned with the Coulombic interactions in particular. They are essencial to the adequate understanding of a vast array of systems, and then for the development science and technology it is crucial to have good simulation techniques for these systems.

When simulating short-ranged potentials we need only to replicate them a few times in the simulation box because the contributions of the replicas vanish rapidly. However, the long-range nature of the electrostatic force prevents the use of simple periodic boundary conditions. There is no distance beyond which the force can be considered negligible, so the simulation box has to interact with infinite replicas of itself if we want to achieve the thermodynamic limit. Beyond that, the calculation depends on the way the replicas are

summed. This means that a conditionally convergent infinite series must be evaluated (for an overall neutral system). If there is a small electric charge in the system, then intrinsic divergences arise, which have to be renormalized [7].

The success of computing these series for neutral systems was first achieved when trying to determine the Madelung constant by calculating the bulk energy of ionic crystals through Ewald Summation methods [8]. The technique has since been improved and extended [9–16]. The main idea behind this algorithm (and our new method) is to separate the potential of a point charge into long contributions, which are calculated in the reciprocal space, and short-range contributions, which are calculated in real space.

Many system of interest - like ionic liquids at electrified interfaces [17–22], charged nanopores [23–25], and nanoconfined electrolytes [26–28] - have a geometry that is a problem for some Ewald techniques that compute part of the energy in Fourier space, and which make a two dimensional transformation of the long range potential that leads to special functions and slow convergence of the series [29, 30].

These systems also exhibit phenomena which could be hard to understand only analytically [31], like charge reversal [32–34], and like-charged attraction [27,35–38]. Techniques have been developed to try to simulate theses systems [16, 39–43].

When we have a system confined by a pair of surfaces, it is difficult to extend the known techniques because of the infinite series that arise from the infinite number of fictional charges. However, methods have been proposed to deal with systems confined by metals or dielectrics [44, 45]. Some methods for simulating metallic surfaces of electrodes rely on minimization procedures to calculate the induced surface charge at every step [18, 44, 46, 47]. There are also methods with electrostatic layer correction, and methods that explicitly sum infinite series of image charges [48–50].

For strongly interacting fluids there are restrictions on the size of the systems which difficult a more accurate investigation. There are approaches that use image charge techniques to sum the series with brute force or using the condition of discontinuity of the displacement vector [48–53]. Some efficient image charge summation for dielectric boundaries have been developed [26]. Despite the difficulties that dense and highly interacting fluids pose (like room temperature ionic liquids), they are promising materials [17, 54], and already have important aplications in supercapacitors [55–58], and renewable energy

devices [59, 60], like solar cells and others [61, 62].

Therefore, with that context in mind, this dissertation proposes a new way to understand the interaction between metal plates inside an electrolyte solution. First we review a 3D Ewald summation technnique (see Chapter 2) in order to understand how this approach can yield the same results of other procedures for the two-dimensional geometry with confining electrified plates, but 10 times faster than usual algorithms. This is important because our new method uses this technique to compute the electrostatic potentials.

Second, we review in Chapter 3 a recent method for charged systems bounded by metallic planar surfaces. We apply the formalism to a lattice model of room temperature ionic liquid [63] and show that our model captures the shape transition in the capacitance curve from camel to bell-shaped [17]. We used Monte Carlo simulations in a constant electrostatic potential ensemble to calculate differential capacitance and ionic density profiles of a Coulomb fluid, both in the electrolyte and ionic liquid regimes. The calculation of electrostatic energy was performed using periodic Green functions. This approach allowed us to easily calculate the induced surface charge on the electrodes.

Third, we review in Section 4.1 a more general system with planar polarizable surfaces. Levin *et al.* [64,65] recently developed and applied this approach that uses periodic Green functions as solutions to the Poisson Equation. The main advantage is that the calculation of the induced charge on the polarizable walls requires only the solution of a linear equation. Also, the ionic interactions can be decoupled from the energy of polarization - for any pair of planar confinement. This decoupling is essencial for the relevance of the algorithm.

Finally, we develop in Chapter 5 a new method for metal plates inside an electrolyte solution which can be seen as an extension of the previous approaches and which shares with them some of the same advantages and particularities of implementation. This can be done because the system can be seen as the general system of Section 4.1 with polarizable surfaces and electrolyte added in the outer regions of the plates.

2 3D Ewald summation of Coulomb systems with slab geometry

This section is based on [7]. A detailed derivation is given in [66]. We consider a system of N particles with charges q^j located at random positions $\boldsymbol{r}^j$ in a simulation box with lengths L_x, L_y and L_z (see Fig. 6). We define the replication vector as $\boldsymbol{r}_{ep} = (m_x L_x, m_y L_y, m_z L_z)$, where $(m_x, m_y, m_z) \in \mathbb{Z}$, to replicate the cell in all directions. The electrostatic potential generated by the ions and all of its replicas at point P located at random position $\boldsymbol{r}$ can be generally written as

$$\phi(\boldsymbol{r}) = \sum_{\boldsymbol{m}}^{\infty} \sum_{j=1}^{N} \int \frac{\rho^j(\boldsymbol{s})}{\epsilon_w |\boldsymbol{r} - \boldsymbol{s}|} d^3\boldsymbol{s} \ , \tag{2.1}$$

where $\rho^j(\boldsymbol{s}) = \mathrm{q}^j \delta(\boldsymbol{s} - \boldsymbol{r}^j - \boldsymbol{r}_{ep})$ is the charge density of q^j and its replicas. An Ewald 3D Summation method is used to handle the conditionally convergent series. The main idea of the algorithm (important for the new method of this Dissertation) is to split the Coulombic potential into a short potential and long-ranged potential that is calculated in Fourier space. A Gaussian charge distribution centered at each particle is added and subtracted, so we have

$$\phi(\boldsymbol{r}) = \sum_{\boldsymbol{m}}^{\infty} \sum_{j=1}^{N} \int \frac{\rho^j(\boldsymbol{s}) - \rho_G^j(\boldsymbol{s})}{\epsilon_w |\boldsymbol{r} - \boldsymbol{s}|} d^3\boldsymbol{s} + \sum_{\boldsymbol{m}}^{\infty} \sum_{j=1}^{N} \int \frac{\rho_G^j(\boldsymbol{s})}{\epsilon_w |\boldsymbol{r} - \boldsymbol{s}|} d^3\boldsymbol{s} \ , \tag{2.2}$$

where $\rho_G^j(\boldsymbol{s}) = \mathrm{q}^j (\kappa_e^3/\sqrt{\pi^3}) \exp\{(-\kappa_e^2 |\boldsymbol{s} - \boldsymbol{r}^j - \boldsymbol{r}_{ep}|^2)\}$ and κ_e is a damping parameter. After rewriting the potential using Error Functions and doing a Fourier transform, we have

$$\phi(\boldsymbol{r}) = \sum_{\boldsymbol{k}=\boldsymbol{0}}^{\infty} \sum_{j=1}^{N} \frac{4\pi \mathrm{q}^j}{\epsilon_w V |\boldsymbol{k}|^2} \exp\left\{ [-\frac{|\boldsymbol{k}|^2}{4\kappa_e^2} + i\boldsymbol{k} \cdot (\boldsymbol{r} - \boldsymbol{r}^j)] \right\} + \sum_{j=1}^{N} \mathrm{q}^j \frac{\mathrm{erfc}(\kappa_e |\boldsymbol{r} - \boldsymbol{r}^j|)}{\epsilon_w |\boldsymbol{r} - \boldsymbol{r}^j|} \ , \tag{2.3}$$

where $\boldsymbol{k} = (\frac{2\pi}{L_x} m_x, \frac{2\pi}{L_y} m_y, \frac{2\pi}{L_z} m_z)$.

There is a divergence from $\boldsymbol{k} = (0, 0, 0)$ which will not be discussed here. Some of the difficulties vanish if the system is charge neutral ($\sum_j \mathrm{q}^j = 0$).

Separating the $\mathbf{k} = \mathbf{0}$ term and putting it in evidence, we can write the renormalized

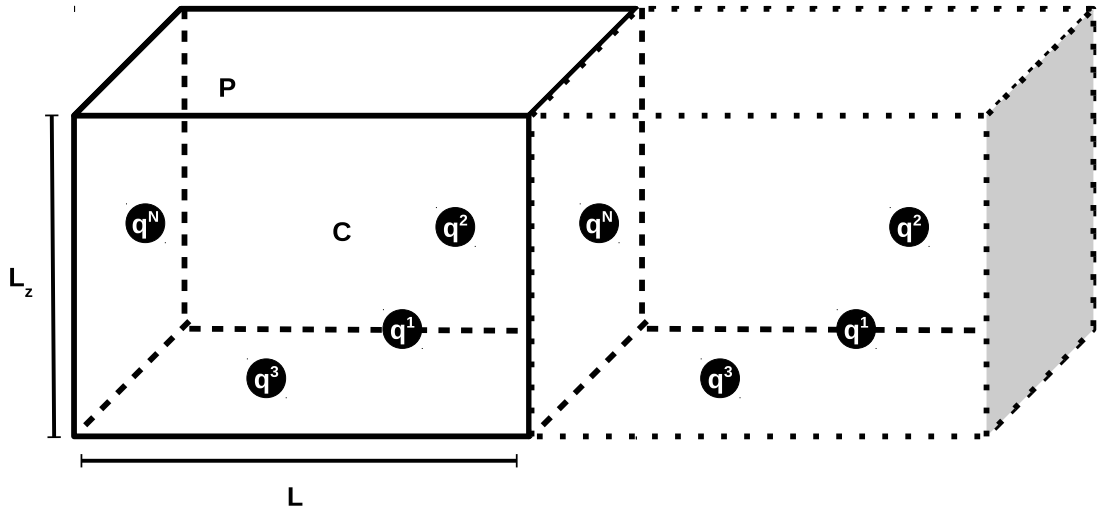

Figure 1: Simulation box with randomly positioned charges and one of its replicas. The origin is located at C (center of the simulation box),and P is a random point [7].

potential as

$$\Delta\phi(\boldsymbol{r}) = \sum_{\boldsymbol{k}\neq\boldsymbol{0}}^{\infty}\sum_{j=1}^{N}\frac{4\pi \mathrm{q}^j}{\epsilon_w V|\boldsymbol{k}|^2}\exp\left\{[-\frac{|\boldsymbol{k}|^2}{4\kappa_e^2}+i\boldsymbol{k}\cdot(\boldsymbol{r}-\boldsymbol{r}^j)]\right\} - \sum_{j=1}^{N}\sum_{n=1}^{3}\frac{2\mathrm{q}^j}{\epsilon_w V\pi^2}B_n(r_n-r_n^j)^2 + \sum_{j=1}^{N}\mathrm{q}^j\frac{\mathrm{erfc}(\kappa_e|\boldsymbol{r}-\boldsymbol{r}^j|)}{\epsilon_w|\boldsymbol{r}-\boldsymbol{r}^j|}\ , \qquad (2.4)$$

where r_n's are components of position vector, and Δ corresponds to the renormalization of the potential in Eq. 2.3. Eq. 2.4 is different from the usual formula found in the literature [9,10,39] for charge neutral isotropic bulk systems. There is a term that depends on the aspect ratios of the macroscopic system (the way the infinite sum is performed), but which has a small contribution from the limit $\mathbf{k}\to\mathbf{0}$ in the calculation of averages on the bulk [16, 43].

For planar geometry we want to replicate the cell only in two out of three directions, x and y, which should be performed infinitely faster than that in z direction for a slab geometry. This condition leads to $B_1 = B_2 = 0$ and $B_3 = \pi^3$. So now Eq. 2.4 is

$$\Delta\phi(\boldsymbol{r}) = \sum_{\boldsymbol{k}\neq\boldsymbol{0}}^{\infty}\sum_{j=1}^{N}\frac{4\pi \mathrm{q}^j}{\epsilon_w V|\boldsymbol{k}|^2}\exp\left\{[-\frac{|\boldsymbol{k}|^2}{4\kappa_e^2}+i\boldsymbol{k}\cdot(\boldsymbol{r}-\boldsymbol{r}^j)]\right\} \qquad (2.5)$$

$$-\sum_{j=1}^{N}\frac{2\pi\mathrm{q}^j}{\epsilon_w V}(r_3-r_3^j)^2 + \sum_{j=1}^{N}\mathrm{q}^j\frac{\mathrm{erfc}(\kappa_e|\boldsymbol{r}-\boldsymbol{r}^j|)}{\epsilon_w|\boldsymbol{r}-\boldsymbol{r}^j|}\ . \qquad (2.6)$$

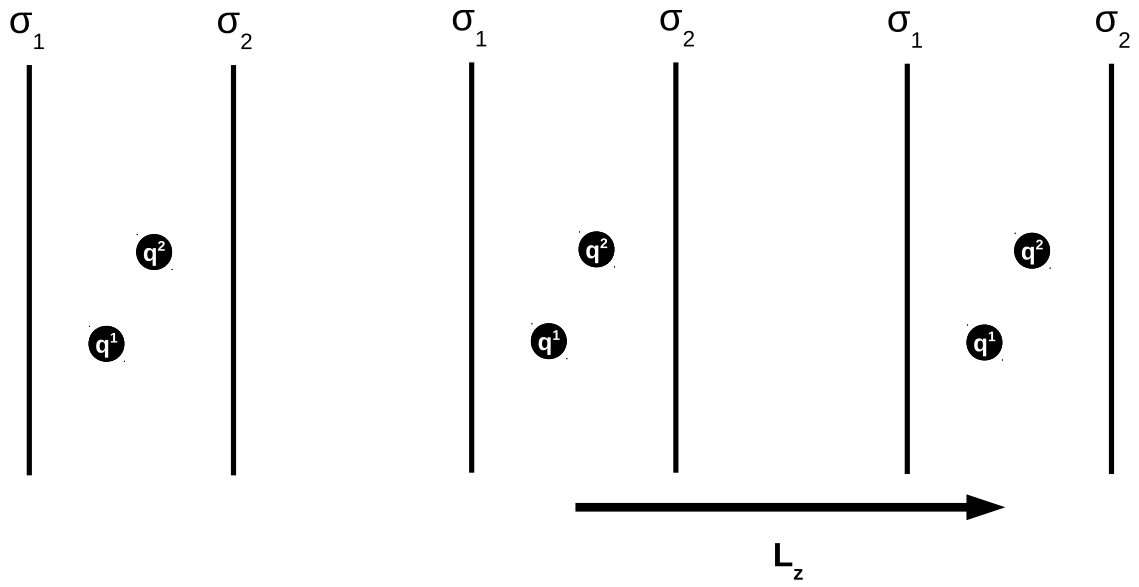

Figure 2: 3D replicated system. The electric fields produced by the z-replication of charged walls cancel out inside the central simulation cell.

A vacuum artificially inserted in the z direction to prevent the replicas in this dimension to add to the total electrostatic potential (see Fig. 9). The empty space must be big enough so the properties of the system can't be altered by the added vacuum.

Now consider the same two particle system than before.The initial random positions of the particles and of the vector $\mathbf{r}$ are limited to $-L_z/4 < z < L_z/4$ so we can introduce the vacuum. The potential difference $\Delta\phi$ can be explicitly calculated using Eq. 2.1 when the simulation cell is replicated only in the x and y directions.

The renormalized electrostatic energy for a non-neutral slab system can now be calculated with $E = \frac{1}{2}\sum_{i=1}^{N} \mathrm{q}^i \Delta\phi(\boldsymbol{r}^i)$, which gives us

$$
\begin{aligned}
E = & \sum_{\boldsymbol{k}\neq\boldsymbol{0}}^{\infty} \frac{2\pi}{\epsilon_w V|\boldsymbol{k}|^2} \exp\left\{[-\frac{|\boldsymbol{k}|^2}{4\kappa_e^2}]\right\}[A(\boldsymbol{k})^2 + B(\boldsymbol{k})^2] \\
& + \frac{2\pi}{\epsilon_w V}[M_z^2 - Q_t G_z] + \frac{1}{2}\sum_{i\neq j}^{N} \mathrm{q}^i\mathrm{q}^j \frac{\mathrm{erfc}(\kappa_e|\boldsymbol{r}^i - \boldsymbol{r}^j|)}{\epsilon_w|\boldsymbol{r}^i - \boldsymbol{r}^j|} \\
& - \frac{\kappa_e}{\epsilon_w\sqrt{\pi}}\sum_{i}^{N} q_i^2 \ , \qquad (2.7)
\end{aligned}
$$

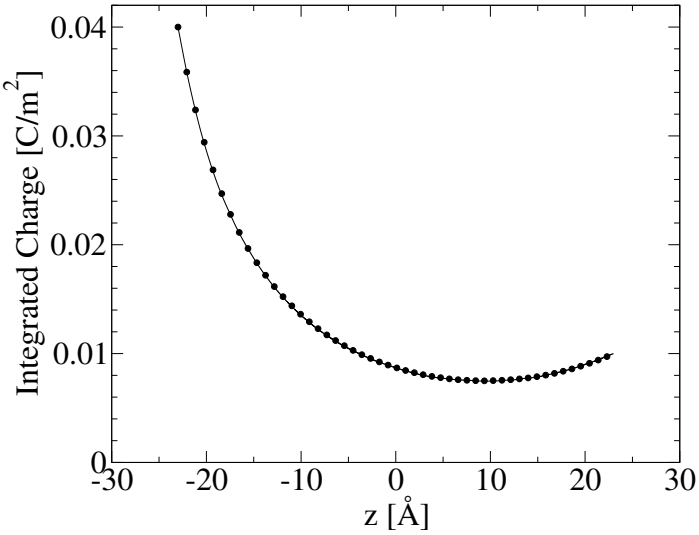

Figure 3: Integrated charge between the plates.The line represents the traditional method [39] and the symbols the modified 3D Ewald approach [7].

where

$$A(\boldsymbol{k}) = \sum_{i=1}^{N} \mathrm{q}^i \cos(\boldsymbol{k} \cdot \boldsymbol{r}^i) \ , \tag{2.8}$$

$$B(\boldsymbol{k}) = -\sum_{i=1}^{N} \mathrm{q}^i \sin(\boldsymbol{k} \cdot \boldsymbol{r}^i) \ , \tag{2.9}$$

$$M_z = \sum_{i=1}^{N} \mathrm{q}^i r_3^i \ , \tag{2.10}$$

$$Q_t = \sum_{i=1}^{N} \mathrm{q}^i \ , \tag{2.11}$$

$$G_z = \sum_{i=1}^{N} \mathrm{q}^i (r_3^i)^2 \ . \tag{2.12}$$

The last term on Eq. 2.7 arises when we carefully double sum the long range potential. For a neutral system ($Q_t = 0$) the earlier expression for the electrostatic energy is recovered [39].

We can give a constant superficial charge to the plates. The resulting field can be treated as an external potential because the electric fields of the transverse replicated plates are constant and cancel out (see Fig. 9).

The main idea of the method is to consider the plates as external potentials instead of a construction of point charges (which slows down the simulations). So the contribution

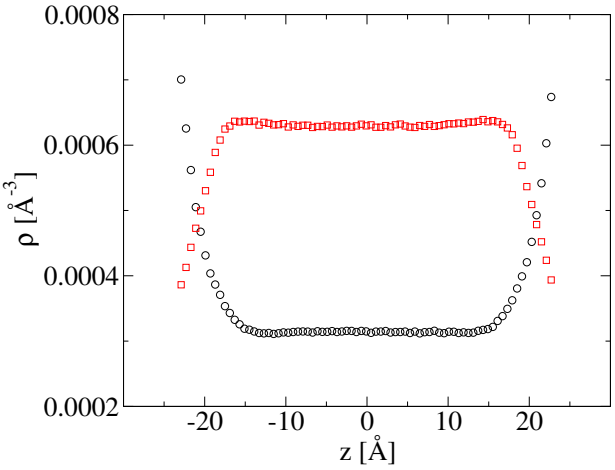

Figure 4: (a) Density profiles of 2 : 1 electrolyte confined by charged infinite walls. Circles are anions and squares are cations.

to the energy becomes

$$E_p = \frac{2\pi}{\epsilon_w} \sum_{i=1}^{N_c} (\sigma_2 - \sigma_1) r_3^i \mathrm{q}^i \ , \tag{2.13}$$

which must be added to Eq. 2.7.

In order to testify the correctness of the method, the authors performed a Metropolis algorithm for nanoconfined ions in slab geometry. Usually it consists of a salt that dissolves in water (Na^+ and Cl^-), so the ions are dissociated in the medium and each has a total electric charge. They performed simulations in the NVT ensemble using the traditional algorithm (plates charged by point particles) and the new method (plates as external potentials).

The results were indistinguishable (see Fig. 8). The computational gain was of one order of magnitude in time in comparison with the corrected 3D Ewald Summation method where the plates are embodied with point charges.

The authors then applied the new method for the case $\sigma_1 = \sigma_2 = 0.04\mathrm{C/m}^2$, which is of practical importance when studying colloidal suspension using Derjaguin approximation [67]. The ionic profiles are shown in Fig. 10. Our new method uses this technique (see Chapter 5).

3 Lattice model of ionic liquid confined by metal electrodes

In this section we briefly review Green functions for ions confined by metal surfaces, and the we discuss Monte Carlo simulations in a constant electrostatic potential ensemble. The results in this section were published in Ref. [63].

3.1 Theory

This section is partially based on the more detailed calculations in Ref. [22]. The electrostatic potential produced by an ion of charge q confined by parallel infinite grounded conducting surfaces located at $z = 0$ and $z = L$ can be written in cylindrical coordinates [75]

$$\phi(\rho, z; z_0) = \frac{4q}{\epsilon L} \sum_{n=1}^{\infty} \sin(k_n z) \sin(k_n z_0) K_0(k_n \rho) \ , \tag{3.1}$$

where $(0, z_0)$ is the coordinate of the ion, (ρ, z) is the observation point, $k_n = n\pi/L$, and K_0 is the modified Bessel function of second type. This expression is difficult to converge when $\rho \to 0$, so find a different representation of the Green function [75]

$$\begin{aligned} &\phi(\rho, z; z_0) = \frac{q}{\epsilon} \int \mathrm{d}k J_0(k\rho) \times \\ &\frac{e^{k|z-z_0|-2kL} + e^{-k|z-z_0|} - e^{-k(z+z_0)} - e^{k(z+z_0)-2kL}}{1 - e^{-2kL}} \ , \end{aligned} \tag{3.2}$$

where J_0 is the Bessel function of order zero, which behaves well when $\rho \to 0$ if $z \neq z_0$.

There is an induced surface charge from the ion between the grounded conducting surfaces, which can be calculated from the discontinuity of the normal component of electric field at the surface. By integration over the surface of each electrode we obtain the induced total surface charge [22]

$$\begin{aligned} Q_l^0 &= -q(1 - \frac{z_0}{L}) \\ Q_r^0 &= -\frac{qz_0}{L} \end{aligned} \tag{3.3}$$

for the left and right electrodes, respectively. If the electrodes are held at a constant potential difference ψ_0 (not grounded), then there is an additional contribution to the

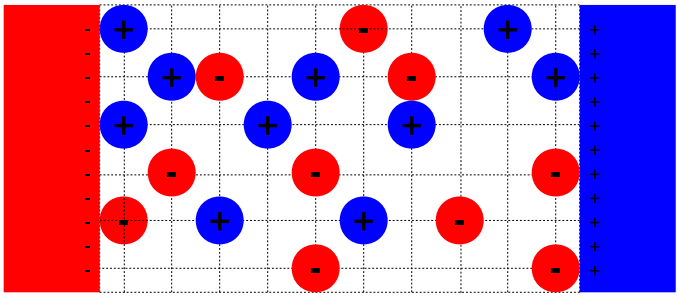

Figure 5: Lattice model of an ionic liquid between two electrodes. Ions are spherical, restricted to move on a lattice. Cations and anions have diameter equal to the lattice spacing.

electrostatic potential

$$\phi_s(z) = \left(\frac{z}{L} - \frac{1}{2}\right)\psi_0 \ . \tag{3.4}$$

The simulations are performed in the NVT ensemble at a fixed electrostatic potential difference ψ between the electrodes [22, 76]. The partition function has the form

$$\mathcal{Z}_\psi = \int \prod_{i=1}^{N} \mathrm{d}\boldsymbol{r}_i \int \mathrm{d}Q e^{-\beta[E(\boldsymbol{r}_1,\ldots,\boldsymbol{r}_N,Q)-\psi Q]} \ , \tag{3.5}$$

where $\beta = 1/k_B T$ and $\mp Q$ is the surface charge on the left and right electrodes, respectively. In this ensemble the surface charge on the electrodes can fluctuate, so the differential capacitance of the system is

$$C = \frac{1}{A}\frac{\partial \langle Q \rangle}{\partial \psi} = \frac{1}{\beta A}\left(\frac{\partial^2 \ln \mathcal{Z}_\psi}{\partial \psi^2}\right) = \frac{\beta}{A}\left[\langle Q^2 \rangle - \langle Q \rangle^2\right] \tag{3.6}$$

where $A = L_x L_y$ is the area of the electrode in the simulation cell, which is periodically replicated in x and y directions.

We need to know the electrostatic energy at a fixed surface charge $E(Q)$ in order to perform simulations in the fixed surface potential ensemble . The charge distribution will not be uniform over the surface of the electrodes, and will respond to the ionic motion.

The electrostatic energy [22] inside the simulation cell for a given surface charge $\pm Q$ is

$$E(Q) = \frac{1}{2}\psi_0 Q + \frac{1}{2}\sum_i q_i \phi(\boldsymbol{r}_i) = \frac{1}{2}\sum_{i\neq j}^{N} q_i G(\boldsymbol{r}_i;\boldsymbol{r}_j) + \sum_{i=1}^{N}\left[U_s(\boldsymbol{r}_i) + \frac{1}{2}q_i\phi_s(z_i)\right] + \frac{1}{2}\psi_0 Q. \tag{3.7}$$

The periodic Green function function constructed using Eq. (3.1)

$$G(\boldsymbol{r};\boldsymbol{r}_0) = \frac{4q}{\epsilon L}\sum_{\boldsymbol{m}=-\infty}^{\infty}\sum_{n=1}^{\infty}\sin(k_n z)\sin(k_n z_0)\times \\ K_0\left(k_n\sqrt{(x-x_0+m_xL_x)^2+(y-y_0+m_yL_y)^2}\right)\ , \tag{3.8}$$

where $\boldsymbol{m}$'s are integers corresponding to periodic replicas of the system. $U_s(\boldsymbol{r}_i)$ is the self energy of each ion calculated using the limiting process,

$$U_s(\boldsymbol{r}_i) = \frac{q_i}{2}\lim_{\rho\to 0}\left[G(\boldsymbol{r}_i;\boldsymbol{r}_i) - \frac{q_i}{\epsilon\rho}\right] \tag{3.9}$$

Using Eq. 3.2, we then obtain [22]

$$U_s(\boldsymbol{r}_i) = \frac{q^2}{2\epsilon}\int \mathrm{d}k \frac{2e^{-2kL} - e^{-2kz_i} - e^{2kz_i-2kL}}{1-e^{-2kL}} + \\ \frac{2q^2}{\epsilon L}\sum_{\boldsymbol{m}\neq\boldsymbol{0}}^{\infty}\sum_{n=1}^{\infty}\sin^2(k_n z_i)K_0\left(k_n\sqrt{m_x^2L_x^2+m_y^2L_y^2}\right)\ . \tag{3.10}$$

The surface potential $\mp\psi_0/2$ on each electrode will fluctuate as a result of ionic motion if the surface charge Q is fixed. The system is charge neutral, so the surface potential for a given surface charge and ionic distribution inside the simulation cell can calculated using Eqs. (3.3) and (3.4). So we have

$$\psi_0 = \frac{4\pi L}{\epsilon A}\left(Q + \sum_{i=1}^{N} q_i\frac{z_i}{L}\right). \tag{3.11}$$

3.2 Monte Carlo Simulations

The simulation cell has volume $V = L_xL_yL$, with $L_x = L_y = 64$Å and $L = 240$Å in the case of symmetric ionic liquids, and $L = 160$Å otherwise. The ionic liquid is confined in the region $-L_x/2 < x < L_x/2$, $-L_y/2 < y < L_y/2$, and $0 < z < L$. The Bjerrum length has the values $\lambda_B = 7.2$Å (appropriate for electrolytes dissolved in pure water at room temperature), and $\lambda_B = 38.4$Å(suitable for RTILs [77, 78]). The ions are constrained to move on a lattice with spacing $a = 4$Å , $a = 8$Å , or $a = 16$Å. We first consider symmetric ionic fluids with spherical ions of diameter equal to the lattice spacing and charge $\pm q$, where q is the proton charge. The compacity factor γ_* is defined by the ratio between

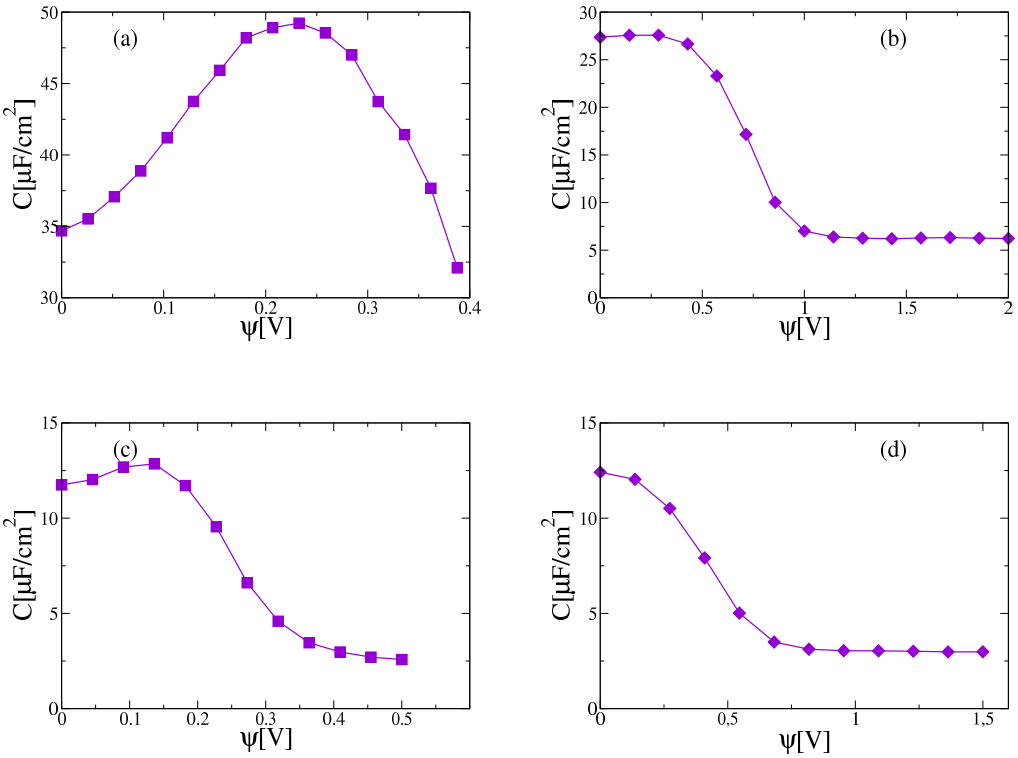

Figure 6: Fig. (a) shows the typical camel-shape curve of the electrolyte capacitance; the parameters are $\lambda_B = 7.2$Å and $\gamma_* = 1/20$ and ion diameter equal to the lattice spacing $a = 8$Å. Fig. (b) shows the typical bell-shape curve of the ionic liquid capacitance; the parameters are $\lambda_B = 38.4$Å and $\gamma_* = 1/2$, and $a = 8$Å. Fig (c) same as (a), but with $a = 16$Å; Fig. (d) same as (b), but with $a = 16$Å. The ions have charge $\pm q$.

lattice sites occupied by the particles and the total available lattice sites in the simulation box (see Fig. 5). The phase space is sampled with short and long-range movements. The differential capacitance is calculated using 4×10^5 uncorrelated samples after equilibrium has been achieved. Fig. 6 shows the change in the form of the differential capacitance between strong and weak coupling regimes. The differential capacitance is symmetric with respect to $\psi \to -\psi$. In the weak coupling electrolyte regime, the differential capacitance has a characteristic camel-back shape, while in the strong coupling regime it has a bell shaped form. The transition between camel-shaped and bell-shaped regimes depends on both γ_* and λ_B (see Fig. 7), and does not occur at the universal value $\gamma_* = 1/3$ (contrary to the predictions of mPB theory [79]).

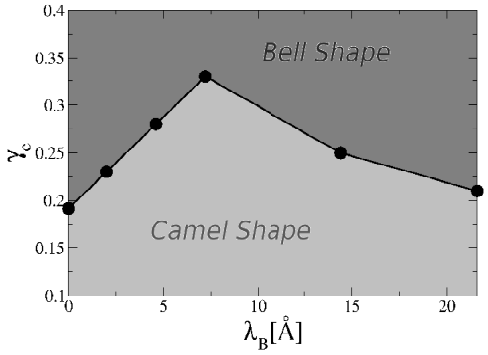

Figure 7: Phase diagram indicating transition between camel-shaped and bell-shaped differential capacitance for size symmetric 1:1 ions of diameter $a = 8\mathring{A}$.

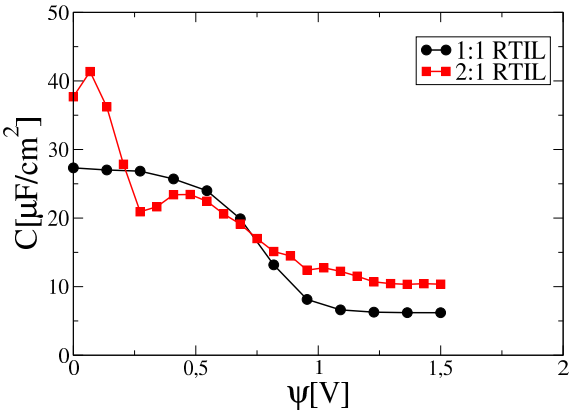

Figure 8: Differential capacitance of 2:1 RTIL for $\gamma_* = 4/10$ contrasted with the capacitance of 1:1 RTIL. The Bjerrum length is 38.4Å. The circles are for 1:1 RTIL, squares corresponds to 2:1 RTIL. The ions have radii 4Å and charges $\mp q$ for 1:1 systems and $2q$ and $-q$ for 2:1 systems.

For ionic liquids (strong coupling regime) with charge asymmetric 2:1 ions, Fig. 8 shows appearance of a second peak at the intermediate applied voltages, if the system is sufficiently dense. This is similar to what has been found in continuum simulations [47]. We see, however, that the height of the secondary peak does not scale with the surface area of the simulation box $A = L_x L_y$, therefore there is no structural phase transition in the local ordering of ions near the electrode, contrary to the suggestion in Ref [47].

Figs. 9 and 10 show that the secondary peak is correlated with the appearance of

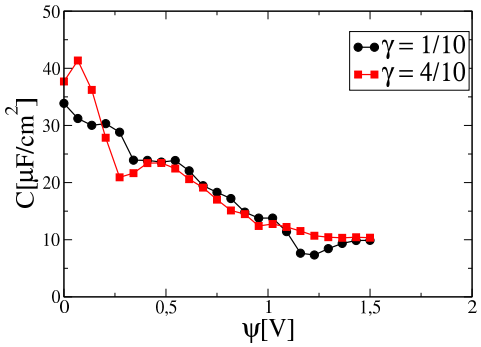

Figure 9: Differential capacitance of 2:1 RTIL, as the compacity γ_* changes. The Bjerrum length is 38.4Å. Circles are for $\gamma_* = 1/10$ and squares for $\gamma_* = 4/10$. The ions have radii 4Å and charges $2q$ and $-q$.

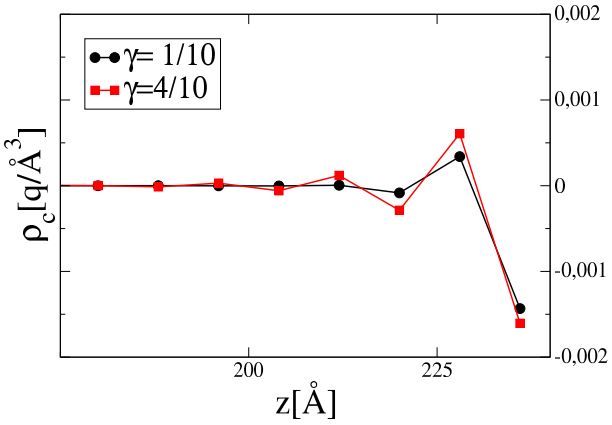

Figure 10: Charge density profiles of 2:1 RTIL near cathode. Potential difference between electrodes is $\psi = 0.5$V. Circles are for compacity $\gamma_* = 1/10$, where the peak is absent; squares are for compacity $\gamma_* = 4/10$.

additional structure in the ionic density profiles. In both cases, we find that the first layer overscreens the charge on the electrode - the charge on the cathode is $\approx -60q$, while the contact layer has charge of $\approx +80q$. Such strong correlational effects clearly can not be captured by mean-field theories (mPB). Finally we consider the differential capacitance

of a 1:1 ionic liquid with size asymmetric (two-to-one) ions (see Fig. 11). Fig. 12 shows that size asymmetry leads to a reduction of the maximum differential capacitance. The magnitude of this reduction is similar to the one found in symmetric systems, with ions of radius $R = 8\mathring{A}$ (Fig. 6).

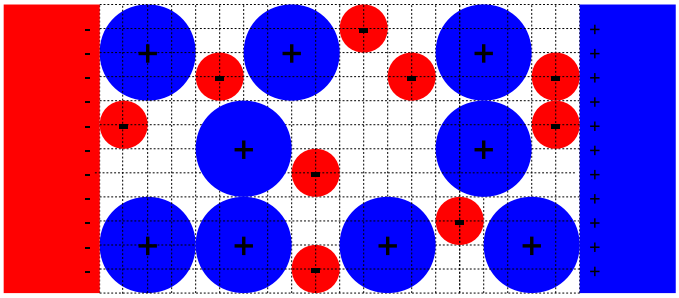

Figure 11: Lattice model of an ionic liquid between two electrodes. Ions are spherical, restricted to move on a lattice. Cations have radius $2a$ and anions a.

The capacitance curve of an asymmetric RTIL has also significantly more structure.

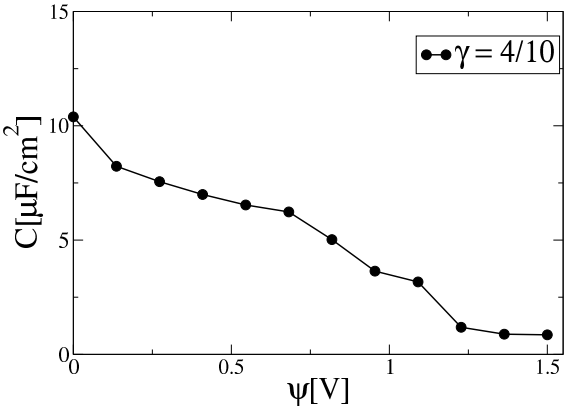

Figure 12: Capacitance curve for size asymmetric 1:1 RTIL. The compacity is $\gamma_* = 4/10$. The cations have radius $R = 2a = 8$Å and anions $R = a = 4$ Å. The Bjerrum length is $\lambda_B = 38.4$Å.

The great advantage of the lattice approach is that it significantly speeds up the simulations by allowing us to precalculate all the interactions. In the limit $a \to 0$, at a fixed ionic size, we should recover the continuum limit. The crossover between lattice and

continuum simulations will be the subject of future work [80].

4 Ionic liquids and general polarizable surfaces

In this section we consider general polarizable surfaces. We firstly analyse a charged fluid confined by polarizable walls in order to obtain a Green function and the energy of the system. Then we calculte the Green function for a system with an infinite metallic plate. In both cases the system is replicated along the x and y axis, generating and infinite periodic charged system.

4.1 Green function for a confined charged fluid

We review here the method recently proposed on [65]. Consider a point particle of charge q_i at position $\mathbf{r}_i = (x_i, y_i, z_i)$ inside a simulation box with sides of lengths L_x, L_y, and L, respectively, in x, y, and z directions.

The infinite periodic charged system is replicated along the x and y, with a finite width L in the z direction. The dielectric constant is ϵ_w in the region $0 < z < L$, and ϵ_c in the regions $z < 0$ and $z > L$ (see Fig. 13). The electrostatic potential at position $\mathbf{r} = (x, y, z)$ satisfies the Poisson equation

$$\nabla^2 G(\mathbf{r}; \mathbf{r}_i) = -\frac{4\pi q_i}{\epsilon_w} \sum_{m_x, m_y = -\infty}^{\infty} \delta(\boldsymbol{r} - \boldsymbol{r}_i + m_x L_x \hat{\boldsymbol{x}} + m_y L_y \hat{\boldsymbol{y}}). \tag{4.1}$$

The periodic delta function can be expressed using Fourier transform representation as

$$\sum_{m_x, m_y = -\infty}^{\infty} \delta(x - x_i + m_x L_x)\delta(y - y_i + m_y L_y) = \frac{1}{L_x L_y} \sum_{\boldsymbol{m} = -\infty}^{\infty} e^{i\left[\frac{2\pi m_x}{L_x}(x - x_i) + \frac{2\pi m_y}{L_y}(y - y_i)\right]}, \tag{4.2}$$

where $\boldsymbol{m} = (m_x, m_y)$. Then the Green function can be written as

$$G(\mathbf{r}; \mathbf{r}_i) = \frac{1}{L_x L_y} \sum_{\boldsymbol{m} = -\infty}^{\infty} g_{\boldsymbol{m}}(z_i, z) e^{i\left[\frac{2\pi m_x}{L_x}(x - x_i) + \frac{2\pi m_y}{L_y}(y - y_i)\right]} \tag{4.3}$$

which is periodic in $\hat{\boldsymbol{x}}$ and $\hat{\boldsymbol{y}}$ directions. Inserting Eq. 4.3 into Eq. 4.1 we have

$$\frac{\partial^2 g_{\boldsymbol{m}}(z_i, z)}{\partial z^2} - k^2 g_{\boldsymbol{m}}(z_i, z) = -\frac{4\pi q_i}{\epsilon_w} \delta(z - z_i) \tag{4.4}$$

where $k = 2\pi\sqrt{m_x^2/L_x^2 + m_y^2/L_y^2}$. The general solution of Eq. 4.4 has the form $Ae^{-kz} + Be^{kz}$. The electrostatic potential must vanish as $z \to \pm\infty$, which restricts this form to a decaying exponential in the outer regions ($z < 0$ and $z > L$). The other boundary conditions are the continuity of potential and discontinuity of displacement vector at the walls.

The symmetry property of Green function, $g_{\boldsymbol{m}}(z_i, z) = g_{\boldsymbol{m}}(z, z_i)$, can be used to account for the singularity of the delta function. The solution to the Dirichlet boundary conditions of the problem can then be written as

$$g_{\boldsymbol{m}}(z_i, z) = \frac{2\pi q_i}{\epsilon_w k(1 - \gamma^2 e^{-2kL})} \times \left[e^{-k|z-z_i|} + \gamma e^{-k(z+z_i)} + \gamma e^{-2kL} e^{k(z+z_i)} + \gamma^2 e^{-2kL} e^{k|z-z_i|}\right] \tag{4.5}$$

where $\gamma = (\epsilon_w - \epsilon_c)/(\epsilon_w + \epsilon_c)$. The surviving terms in the $\boldsymbol{m}$ summation are just the cosine functions, so the potential assumes the form

$$G(\mathbf{r}; \mathbf{r}_i) = \frac{1}{L_x L_y} \sum_{\boldsymbol{m}} g_{\boldsymbol{m}}(z_i, z) \cos\left[\frac{2\pi m_x}{L_x}(x - x_i) + \frac{2\pi m_y}{L_y}(y - y_i)\right] . \tag{4.6}$$

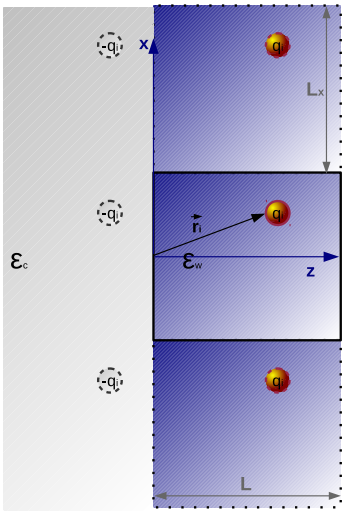

Figure 13: Representation of a system with only one boundary with Dirichlet and Neumann conditions. Only the first two images of the main simulation box in the x direction are shown. [65]

4.2 Energy of the confined charged fluid

This section is based on Ref. [65]. The total energy for a system of N periodically replicated charged particles is given by

$$U = \sum_{i=1}^{N} \sum_{j=1}^{N} \frac{q_j}{2} G(\mathbf{r}_j; \mathbf{r}_i). \tag{4.7}$$

The total energy can be split into the polarization and direct Coulomb contributions

$$U = U_{Ew} + U_p, \tag{4.8}$$

where U_{Ew} is the direct Coulomb contribution,

$$U_{Ew} = \sum_{i=1}^{N} \sum_{j=1}^{N} q_j \frac{G_0(\mathbf{r}_j; \mathbf{r}_i)}{2}, \tag{4.9}$$

which can be calculated using the modified 3d Ewald Summation method (see Chapter 2). The energy U_p due to surface polarizability can be rewritten as

$$\begin{aligned} U_p =& U_\gamma + \frac{\pi}{\epsilon_w L_d^2} \sum_{\boldsymbol{m}'} \frac{\gamma}{k(1-\gamma^2 e^{-2kL})} \times \\ & \{f_1(\boldsymbol{m})^2 + f_2(\boldsymbol{m})^2 + e^{-2kL}\left(f_3(\boldsymbol{m})^2 + f_4(\boldsymbol{m})^2\right) + 2\gamma e^{-2kL}[f_3(\boldsymbol{m}) f_1(\boldsymbol{m}) + f_2(\boldsymbol{m}) f_4(\boldsymbol{m})]\}\ , \end{aligned} \tag{4.10}$$

where $L_x = L_y = L_d$ are set without loss of generality. The number of integers (m_x, m_y) necessary to obtain a converged energy depend on the lateral size of the simulation box L_d. The contribution U_γ arises from the $k \to 0$ limit, and is zero if $\gamma \in (-1, 1)$. For $\gamma = -1$ and $\gamma = +1$ it is

$$U_{(-1)} = -\frac{2\pi}{L_d^2}\left[\frac{M_z^2}{L} - Q_t M_z\right], \tag{4.11}$$

$$U_{(+1)} = -\frac{2\pi Q_t}{L_d^2}\left[M_z - \frac{\Omega_z}{L}\right], \tag{4.12}$$

where

$$Q_t = \sum_{i=1}^{N} q_i \tag{4.13}$$

$$M_z = \sum_{i=1}^{N} q_i z_i \tag{4.14}$$

$$\Omega_z = \sum_{i=1}^{N} q_i z_i^2. \tag{4.15}$$

The $f_i(\boldsymbol{m})$ functions are defined as

$$f_1(\boldsymbol{m}) = \sum_{i=1}^{N} q_i \cos\left[\frac{2\pi}{L_d}(m_x x_i + m_y y_i)\right] e^{-kz_i} \ , \tag{4.16}$$

$$f_2(\boldsymbol{m}) = \sum_{i=1}^{N} q_i \sin\left[\frac{2\pi}{L_d}(m_x x_i + m_y y_i)\right] e^{-kz_i} \ , \tag{4.17}$$

$$f_3(\boldsymbol{m}) = \sum_{i=1}^{N} q_i \cos\left[\frac{2\pi}{L_d}(m_x x_i + m_y y_i)\right] e^{kz_i} \ , \tag{4.18}$$

$$f_4(\boldsymbol{m}) = \sum_{i=1}^{N} q_i \sin\left[\frac{2\pi}{L_d}(m_x x_i + m_y y_i)\right] e^{kz_i} \ . \tag{4.19}$$

If there is a surface charge present at the interfaces, it can be included as an external potential [68]

$$U_{sur} = -\frac{2\pi(\sigma_1 - \sigma_2)}{\epsilon_w} \sum_{i=1}^{N} q_i z_i \ , \tag{4.20}$$

where σ_1 and σ_2 are the surface charge densities at $z = 0$ and $z = L$, respectively.

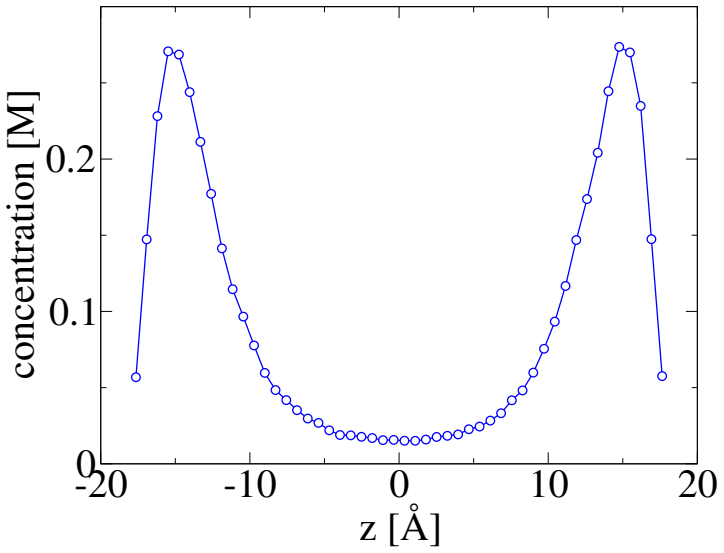

Figure 14: Density profile of trivalent counterions confined between charged dielectric surfaces, $\gamma = 0.95$. The surfaces charge densities are -0.05 C/m^2. The line is a guide to the eyes.

In Fig. 14 there is the density profile of trivalent counterions confined between charged dielectric surfaces of $\gamma = 0.95$. The confining surfaces are separated by a distance $L =$

40 Å. The number of counterions is $N_c = 100$ and the surfaces are equally charged with charge density -0.05 C/m^2. We see a strong repulsion of ions from the interface produced by the induced surface charge. This result is in agreement with an earlier image charge algorithm [26].

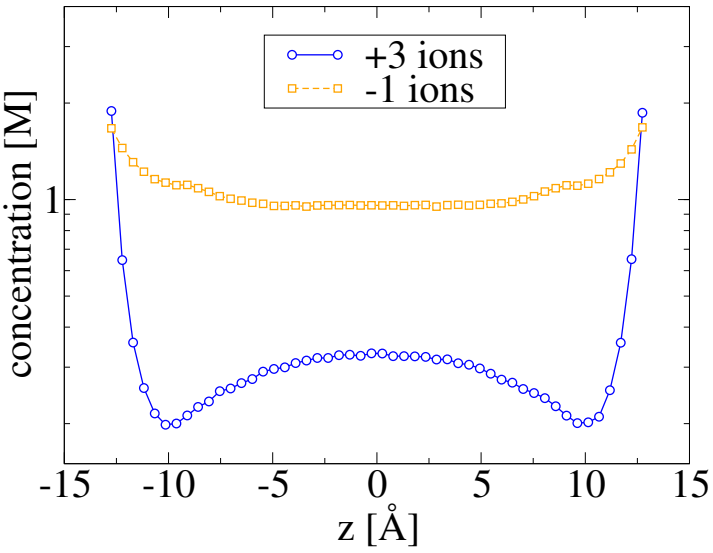

Figure 15: Density profiles of cations and anions confined between grounded metal plates, $\gamma = -1$. The $3:1$ salt concentration is 0.35 M. The lines are guides to the eye.

In Fig. 15 there is the density profiles of cations and anions of a dissolved 3:1 electrolyte at concentration 0.35 M, confined by grounded metal electrodes, $\gamma = -1$, separated by distance $L = 30$ Å. Instead of the repulsion of the previous case, we see the expected attraction of charges to the metal electrodes. This effect can be understood considering the image charges of opposite sign induced inside the electrodes.

4.3 Green function for a metallic plate

The system with a metallic plate at $z = 0$ with periodic replicas in x and y and a point charge q_i at $\boldsymbol{r} = (0, 0, z_i)$ can be handled the same way. Here we have to solve

$$\frac{\partial^2 g_{\boldsymbol{m}}(z; z_i)}{\partial z^2} - k^2 g_{\boldsymbol{m}}(z; z_i) = -\frac{4\pi q_i}{\epsilon_\omega}\delta(z - z_i), \tag{4.21}$$

where we used the first Maxwell equation and expanded the deltas of x and y with complex exponentials. Similarly to the previous subsection, the solutions are simple exponentials.

We first write the function to the region to the left of the charge as

$$g_{\boldsymbol{m},<}(z;z_i) = \begin{cases} Ae^{-kz_<} + Be^{+kz_<} & ,0 < z < z_i \\ De^{+kz_<} & ,z < 0 \end{cases} \tag{4.22}$$

From the boundary value problem at the plate we have $A + B = D$ and $A = \gamma B$, where

$$\gamma = \frac{\epsilon_w - \epsilon_m}{\epsilon_w + \epsilon_m}. \tag{4.23}$$

For metals, $\gamma = -1$. For the region to the right of the charge we have

$$g_{\boldsymbol{m},>}(z;z_i) = Ce^{-kz_>}. \tag{4.24}$$

From the symmetry of the Green function, $g_{\boldsymbol{m}}(z;z_i) = g_{\boldsymbol{m}}(z_i;z)$ and we have

$$g_{\boldsymbol{m}}(z;z_i) = A^{'}\left(e^{-kz_<} + \frac{1}{\gamma}e^{+kz_<}\right)\left(e^{-kz_>}\right). \tag{4.25}$$

We then integrate Eq. 4.21 from $(z_i - \epsilon)$ to $(z_i + \epsilon)$ with $\epsilon \to 0$. So now we have to solve

$$A^{'}k\left[\left(e^{-kz_i} + \frac{1}{\gamma}e^{+kz_i}\right)\left(-e^{-kz_i}\right) - \left(-e^{-kz_i} + \frac{1}{\gamma}e^{+kz_i}\right)\left(e^{-kz_i}\right)\right] = -\frac{4\pi q_i}{\epsilon_w}. \tag{4.26}$$

After solving we have

$$A^{'} = \frac{2\pi q_i \gamma}{k\epsilon_w}. \tag{4.27}$$

Then the total Green function is

$$G(\boldsymbol{r};\boldsymbol{r_i}) = \frac{2\pi q_i}{\epsilon_\omega L_x L_y}\sum_{\boldsymbol{m}}\frac{1}{k}\left[\gamma e^{-k(z+z_i)} + e^{-k|z-z_i|}\right] cos\left[\frac{2\pi m_x}{L_x}(x - x_i) + \frac{2\pi m_y}{L_y}(y - y_i)\right] \tag{4.28}$$

5 Metal surfaces inside an electrolyte solution

In this section we develop the main algorithm which allows us to simulate metal plates inside an electrolyte. The system is ilustrated in Fig. 16. This kind of system hasn't been studied much due to the problem of dealing with the rearrangement of surface charges that occurs when the plates are in an electrolyte. As we will see, the methods reviewed in the Appendices, together with the inclusion of surface potentials, allow us to develop an efficient approach to this problem. We start by obtaining Green functions for each region.

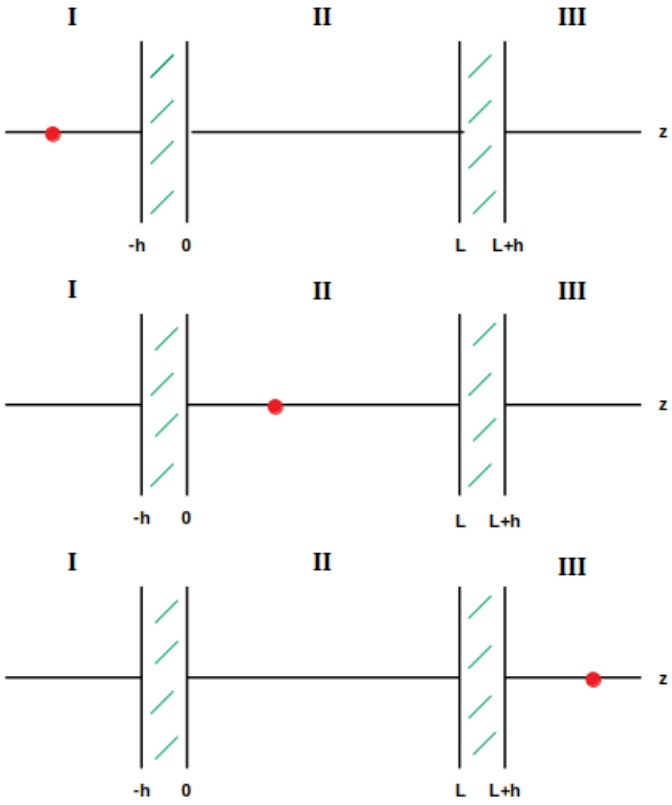

Figure 16: Representations of a system with planar metal surfaces inside an electrolyte. The red dots are point charges.

5.1 Green functions

In this section we calculate the total Green function G for grounded slabs at zero potential. The general form is given by (see Chapter 4)

$$G(\boldsymbol{r};\boldsymbol{r_i}) = \frac{1}{L_x L_y}\sum_{\boldsymbol{m}} g_{\boldsymbol{m}}(z_i,z) cos\left[\frac{2\pi m_x}{L_x}(x-x_i)+\frac{2\pi m_y}{L_y}(y-y_i)\right], \tag{5.1}$$

where $g_{\boldsymbol{m}}(z_i,z)$ is specific to each region.

The total electrostatic potential in each region is rewritten as

$$G(\mathbf{r};\mathbf{r}_i) = [G(\mathbf{r};\mathbf{r}_i) - G_0(\mathbf{r};\mathbf{r}_i)] + G_0(\mathbf{r};\mathbf{r}_i) \tag{5.2}$$

We also define $\tilde{G}(\mathbf{r};\mathbf{r}_i) = G(\mathbf{r};\mathbf{r}_i) - G_0(\mathbf{r};\mathbf{r}_i)$ as the polarization contribution to the total Green function.

The electrostatic potential $G_0(\boldsymbol{r};\boldsymbol{r_i})$ diverges in the limit $k \to 0$, when m_x,$m_y \to 0$. This divergence can be renormalized, but the remaining sum is still slowly convergent. However, $G_0(\boldsymbol{r};\boldsymbol{r_i})$ can be efficiently calculated using a modified 3D Ewald summation technique [39,68] or other methods [29,50]. The details of the 3D Ewald Summation that we used are reviewed in the Chapter 2.

The final expressions are written as

$$G(\boldsymbol{r};\boldsymbol{r_i}) = G_0(\boldsymbol{r};\boldsymbol{r_i}) + G_{(\gamma)}(\boldsymbol{r};\boldsymbol{r_i}) + \tilde{G}'(\boldsymbol{r};\boldsymbol{r_i}), \tag{5.3}$$

where the prime on $\tilde{G}'(\boldsymbol{r};\boldsymbol{r_i})$ excludes the $m_x = m_y = 0$ term in the summation of $\tilde{G}(\boldsymbol{r};\boldsymbol{r_i})$, and for our system we have $\gamma = -1$. With that we can now evaluate the functions for each region.

5.1.1 Source charge on region I

For this region of the system ($z < -h$), the problem is analogous to the one in the Section 4.3, but with the plate moved to $z = -h$ and q_i at $z_i < -h$. The term $g_{\boldsymbol{m}}(z_i,z)$ on Eq. 5.1.2 is given by

$$g_{\boldsymbol{m}}(z_i,z) = \frac{2\pi q_i}{\epsilon_\omega L_x L_y}\frac{\gamma e^{-k(-z-z_i+h)} + e^{-k|z-z_i+h|}}{k}. \tag{5.4}$$

For $\gamma \to 0$, Eq. 5.1.2 becomes

$$G_0(\boldsymbol{r};\boldsymbol{r_i}) = \frac{2\pi q_i}{\epsilon_\omega L_x L_y}\sum_{\boldsymbol{m}}\frac{e^{-k|z-z_i+h|}}{k} cos\left[\frac{2\pi m_x}{L_x}(x-x_i)+\frac{2\pi m_y}{L_y}(y-y_i)\right]. \tag{5.5}$$

The polarization contribution is given by

$$\tilde{G}(\boldsymbol{r};\boldsymbol{r_i}) = \frac{2\pi q_i}{\epsilon_\omega L_x L_y} \sum_{\boldsymbol{m}} \frac{\gamma e^{-k(-z-z_i+h)}}{k} cos\left[\frac{2\pi m_x}{L_x}(x-x_i) + \frac{2\pi m_y}{L_y}(y-y_i)\right]. \tag{5.6}$$

For $\gamma = -1$ (metals) the $m_x = m_y = 0$ term contains an infinite constant and a finite function of z,

$$\frac{2\pi q_i}{\epsilon_w L_x L_y}\left[-\frac{1}{k} + (-z-z_i+h) + \mathcal{O}(k)\right]. \tag{5.7}$$

The infinite constant is neglected again, and we write

$$G_{(-1)}(\boldsymbol{r};\boldsymbol{r_i}) = -\frac{2\pi q_i}{\epsilon_\omega L_x L_y}(z+z_i-h). \tag{5.8}$$

The final expression for the total electrostatic potential can now be written as Eq. 5.3.

5.1.2 Source charge on region II

For this region of the system ($0 < z < L$) the term $g_{\boldsymbol{m}}(z_i, z)$ on Eq. is given by (see Section 4.1)

$$g_{\boldsymbol{m}}(z_i,z) = \frac{2\pi q_i}{\epsilon_\omega k(1-\gamma^2 e^{-2kL})}\left[e^{-k|z-z_i|} + \gamma e^{-k(z+z_i)} + \gamma e^{-2kL}e^{k(z+z_i)} + \gamma^2 e^{-2kL}e^{k|z-z_i|}\right]. \tag{5.9}$$

In the absence of dielectric contrast ($\gamma \to 0$) Eq. 5.1.2 reduces to

$$G_0(\mathbf{r};\mathbf{r}_i) = \frac{2\pi q_i}{\epsilon_w L_x L_y} \sum_{\boldsymbol{m}=-\infty}^{\infty} \frac{e^{-k|z-z_i|}}{k} \cos\left[\frac{2\pi m_x}{L_x}(x-x_i) + \frac{2\pi m_y}{L_y}(y-y_i)\right], \tag{5.10}$$

which is a representation of the electrostatic potential produced by a periodically replicated point charge in the x and y directions. The polarization contribution is then given by

$$\begin{aligned}\tilde{G}(\mathbf{r};\mathbf{r}_i) =& \frac{2\pi q_i}{\epsilon_w L_x L_y} \sum_{\boldsymbol{m}=-\infty}^{\infty} \frac{1}{k(1-\gamma^2 e^{-2kL})} \\ &\times \left[\gamma e^{-k(z+z_i)} + \gamma e^{-2kL}e^{k(z+z_i)} + 2\gamma^2 e^{-2kL}\cosh\left(k(z-z_i)\right)\right] \\ &\times \cos\left[\frac{2\pi m_x}{L_x}(x-x_i) + \frac{2\pi m_y}{L_y}(y-y_i)\right].\end{aligned} \tag{5.11}$$

The limit $k \to 0$ ($m_x = m_y = 0$) requires additional care and requires renormalization procedures. The calculations are separated in three cases: $\gamma = +1$, $\gamma = -1$ and $\gamma \in$

$(-1, 1)$. For our metallic system we are interested in $\gamma = -1$, but we will review the other cases. For $-1 < \gamma < 1$ the $m_x = m_y = 0$ term diverges as

$$-\frac{4\pi q_i}{\epsilon_w L_x L_y}\left[\frac{\gamma}{k(\gamma-1)} + \frac{\gamma L}{(\gamma-1)^2} + \mathcal{O}(k)\right] . \tag{5.12}$$

Since this is a constant (independent of position), it will not contribute to the force and can be renormalized away. For $\gamma = -1$ the $m_x = m_y = 0$ term contains an infinite constant and a finite function of z,

$$\frac{2\pi q_i}{\epsilon_w L_x L_y}\left[-\frac{1}{k} + (z + z_i - 2\frac{z_i z}{L}) + \mathcal{O}(k)\right] . \tag{5.13}$$

The infinite constant is neglected again, and we write

$$G_{(-1)}(\mathbf{r}; \mathbf{r}_i) = \frac{2\pi q_i}{\epsilon_w L_x L_y}(z + z_i - 2\frac{z_i z}{L}) \tag{5.14}$$

For $\gamma = +1$ we have

$$\frac{2\pi q_i}{\epsilon_w L_x L_y}\left[\frac{2}{Lk^2} - \frac{1}{k} + \frac{2L^2 - 3L(z+z_i) + 3(z^2+z_i^2)}{3L} + \mathcal{O}(k)\right] , \tag{5.15}$$

so that

$$G_{(+1)}(\mathbf{r}; \mathbf{r}_i) = \frac{2\pi q_i}{\epsilon_w L_x L_y}\left[-(z + z_i) + \frac{z^2 + z_i^2}{L}\right] . \tag{5.16}$$

The final expression for the total electrostatic potential can now be written as Eq. 5.3, which makes evident the contribution of the polarized walls. Furthermore, this polarization part is decoupled of the periodic ionic contribution.

5.1.3 Source charge on region III

For this region of the system ($z > L + h$) the problem is the same as the one in the Section 4.3, but with the plate moved to $z = L + h$ and q_i at $z_i > L + h$. The term $g_{\boldsymbol{m}}(z_i, z)$ on Eq. 5.1.2 is given by

$$g_{\boldsymbol{m}}(z_i, z) = \frac{2\pi q_i}{\epsilon_\omega L_x L_y}\frac{\gamma e^{-k(z+z_i-L-h)} + e^{-k|z-z_i-L-h|}}{k}. \tag{5.17}$$

For $\gamma \to 0$, Eq. 5.1.2 becomes

$$G_0(\boldsymbol{r}; \boldsymbol{r_i}) = \frac{2\pi q_i}{\epsilon_\omega L_x L_y}\sum_{\boldsymbol{m}}\frac{e^{-k|z-z_i-L-h|}}{k} cos\left[\frac{2\pi m_x}{L_x}(x - x_i) + \frac{2\pi m_y}{L_y}(y - y_i)\right] \tag{5.18}$$

The polarization contribution is given by

$$\tilde{G}(\boldsymbol{r};\boldsymbol{r_i}) = \frac{2\pi q_i}{\epsilon_\omega L_x L_y} \sum_{\boldsymbol{m}} \frac{\gamma e^{-k(z+z_i-L-h)}}{k} cos\left[\frac{2\pi m_x}{L_x}(x-x_i) + \frac{2\pi m_y}{L_y}(y-y_i)\right] \tag{5.19}$$

For $\gamma = -1$ the $m_x = m_y = 0$ term contains an infinite constant and a finite function of z,

$$\frac{2\pi q_i}{\epsilon_w L_x L_y}\left[-\frac{1}{k} + (z + z_i - h - L) + \mathcal{O}(k)\right]. \tag{5.20}$$

The infinite constant is neglected again, and we write

$$G_{(-1)}(\boldsymbol{r};\boldsymbol{r_i}) = \frac{2\pi q_i}{\epsilon_\omega L_x L_y}(z + z_i - h - L). \tag{5.21}$$

The final expression for the total electrostatic potential can now be written as Eq. 5.3.

5.2 Surface potentials from added charges

The Green function in Section 4.1 was calculated with the boundary conditions of zero potential. This is not correct for what we want because we have different boundary conditions for the plates, which require us to add surface charges to keep the slabs neutral. The charges will be on each face of the two slabs (see Fig. 16). We want to calculate the potential Φ produced by this charge distribution. Once we add the potential due to surface charges, the slabs will no longer be at zero potential. If we label the surfaces from 1 to 4 from left to right and we refer to the left plate as L and the right plate as R, then have the conditions

$$\begin{aligned} \sigma_1 + \sigma_2 &= \sigma_L, \\ \sigma_3 + \sigma_4 &= \sigma_R, \\ \sigma_1 &= \sigma_2 + \sigma_3 + \sigma_4, \\ \sigma_4 &= \sigma_1 + \sigma_2 + \sigma_3. \end{aligned} \tag{5.22}$$

The induced charges are

$$\begin{cases} \sigma_L &= \frac{q}{A}\frac{(L-z_i)}{L}, \\ \sigma_R &= \frac{q}{A}\frac{z_i}{L}. \end{cases} \tag{5.23}$$

From Eqs. 5.22 and 5.23 we have

$$q_i \text{ on region II} \begin{cases} \sigma_1 &= \sigma_4 = +\frac{q}{2A} \\ \sigma_2 &= -\sigma_3 = +\frac{q}{2A}\left(1 - \frac{2z_i}{L}\right) \end{cases} \tag{5.24}$$

$$q_i \text{ on region I} \begin{cases} \sigma_1 &= \sigma_4 = +\frac{q}{2A} \\ \sigma_2 &= -\sigma_3 = +\frac{q}{2A} \end{cases} \tag{5.25}$$

$$q_i \text{ on region III} \begin{cases} \sigma_1 &= \sigma_4 = +\frac{q}{2A} \\ \sigma_2 &= -\sigma_3 = -\frac{q}{2A} \end{cases} \tag{5.26}$$

Each region j will have three surface potentials given by

$$\Phi_{I,j} = +\frac{2\pi}{\epsilon}(\sigma_1 + \sigma_4)(z + h) + \Psi_{I,j}, \tag{5.27}$$

$$\Phi_{II,j} = -\frac{2\pi}{\epsilon}(\sigma_2 - \sigma_3)(z - \frac{L}{2}) + \Psi_{II,j}, \tag{5.28}$$

$$\Phi_{III,j} = -\frac{2\pi}{\epsilon}(\sigma_1 + \sigma_4)(z - L - h) + \Psi_{III,j}, \tag{5.29}$$

where $\Psi_{I,j}$, $\Psi_{II,j}$ and $\Psi_{III,j}$ are constants. From the continuity of the potentials, we have

$$\Phi_{I,j}(z = -h) = \Phi_{II,j}(z = 0), \tag{5.30}$$

$$\Phi_{II,j}(z = L) = \Phi_{III,j}(z = L + h). \tag{5.31}$$

So we start with the source on region II and impose $\Phi_{II,2}(z = \frac{L}{2}) = 0$. That gives us $\Psi_{II,2} = 0$. Then from the continuity of the potentials we obtain

$$\Psi_{I,2} = -\frac{2\pi q_i}{\epsilon A}\left(z_i - \frac{L}{2}\right), \tag{5.32}$$

$$\Psi_{III,2} = \frac{2\pi q_i}{\epsilon A}\left(z_i - \frac{L}{2}\right). \tag{5.33}$$

Then, with the source on region I, we use the symmetries (Eq. 5.30) with region II to obtain $\Psi_{II,1} = \frac{2\pi q_i}{\epsilon A}(z_i + h)$. Then from the continuity of the potentials we obtain the other two constants

$$\Psi_{I,1} = \frac{2\pi q_i}{\epsilon A}\left(z_i + h + \frac{L}{2}\right), \tag{5.34}$$

$$\Psi_{III,1} = \frac{2\pi q_i}{\epsilon A}\left(z_i + h - \frac{L}{2}\right). \tag{5.35}$$

Then we repeat the procedure with the source on region III, obtaining

$$\Psi_{I,3} = \frac{2\pi q_i}{\epsilon A}\left(-z_i + h + \frac{L}{2}\right), \tag{5.36}$$

$$\Psi_{II,3} = \frac{2\pi q_i}{\epsilon A}\left(-z_i + h + L\right), \tag{5.37}$$

$$\Psi_{III,3} = -\frac{2\pi q_i}{\epsilon A}\left(z_i - h - \frac{3L}{2}\right). \tag{5.38}$$

The total potential on each region has the form

$$G_t(\mathbf{r};\mathbf{r}_i) = G(\mathbf{r};\mathbf{r}_i) + \Phi(\mathbf{r};\mathbf{r}_i), \tag{5.39}$$

where $G(\mathbf{r};\mathbf{r}_i)$ is the total electrostatic potential calculated before.

The Green functions have to be symmetric across all regions. So G_t must be symmetric when we exchange the source and observation points. Since G is different for the three regions, this is a much more stringent test of the validity of our calculations. The Green function exists only in the region where there is charge, so when we try to test the symmetry between different regions this will mean symmetry between the surface potentials Φ.

After checking the boundaries and symmmetries, we can summarize the surface potentials as

$$q_i \text{ on region I} \begin{cases} \Phi_I & = +\frac{2\pi q_i}{\epsilon A}(z + z_i + 2h + \frac{L}{2}) \\ \Phi_{II} & = -\frac{2\pi q_i}{\epsilon A}(z - z_i - h - \frac{L}{2}) \\ \Phi_{III} & = -\frac{2\pi q_i}{\epsilon A}(z - z_i - 2h - \frac{L}{2}) \end{cases} \tag{5.40}$$

$$q_i \text{ on region II} \begin{cases} \Phi_I & = +\frac{2\pi q_i}{\epsilon A}(z - z_i + h + \frac{L}{2}) \\ \Phi_{II} & = -\frac{2\pi q_i}{\epsilon A}(z + z_i - \frac{zz_i}{L/2} - \frac{L}{2}) \\ \Phi_{III} & = -\frac{2\pi q_i}{\epsilon A}(z - z_i - h - \frac{L}{2}) \end{cases} \tag{5.41}$$

$$q_i \text{ on region III} \begin{cases} \Phi_I & = +\frac{2\pi q_i}{\epsilon A}(z - z_i + 2h + \frac{L}{2}) \\ \Phi_{II} & = +\frac{2\pi q_i}{\epsilon A}(z - z_i + h + \frac{L}{2}) \\ \Phi_{III} & = -\frac{2\pi q_i}{\epsilon A}(z + z_i - 2h - \frac{5L}{2}) \end{cases} \tag{5.42}$$

5.3 Energies

The analysis in this section is similar to the one in Section 4.2. The total energy for this system of N periodically replicated charged particles is given by

$$U = \sum_{i=1}^{N} \sum_{j=1}^{N} q_j \frac{G_t(\boldsymbol{r_j}; \boldsymbol{r_i})}{2}, \tag{5.43}$$

We can split the total energy into the polarization, the direct Coulomb contributions and and extra term U_Φ to account for the surface potentials,

$$U = U_{Ew} + U_p + U_\Phi, \tag{5.44}$$

where U_{Ew} is the direct Coulomb contribution,

$$U_{Ew} = \sum_{i=1}^{N} \sum_{j=1}^{N} q_j . \frac{G_0(\boldsymbol{r_j}; \boldsymbol{r_i})}{2}, \tag{5.45}$$

which can be calculated using the modified 3d Ewald Summation method (see Chapter 2). The energy U_p can be written as

$$U_p = U_\gamma + U_{p'}, \tag{5.46}$$

where $\gamma = -1$, and the prime on $U_{p'}$ excludes the $m_x = m_y = 0$ term in the summation. So for each region U will be calculated as

$$U = U_{Ew} + U_{p'} + U_{(-1)} + U_\Phi. \tag{5.47}$$

We set $L_x = L_y = L_d$ without loss of generality. The number of integers (m_x, m_y) necessary to obtain a converged energy depend on the lateral size of the simulation box L_d. The $f_i(\boldsymbol{m})$ functions are again defined as

$$f_1(\boldsymbol{m}) = \sum_{i=1}^{N} q_i cos \left[\frac{2\pi}{L_d} (m_x x_i + m_y y_i) \right] e^{-kz_i}, \tag{5.48}$$

$$f_2(\boldsymbol{m}) = \sum_{i=1}^{N} q_i sin \left[\frac{2\pi}{L_d} (m_x x_i + m_y y_i) \right] e^{-kz_i}, \tag{5.49}$$

$$f_3(\boldsymbol{m}) = \sum_{i=1}^{N} q_i cos \left[\frac{2\pi}{L_d} (m_x x_i + m_y y_i) \right] e^{kz_i}, \tag{5.50}$$

$$f_4(\boldsymbol{m}) = \sum_{i=1}^{N} q_i sin \left[\frac{2\pi}{L_d} (m_x x_i + m_y y_i) \right] e^{kz_i}. \tag{5.51}$$

For the whole system we define

$$Q_t = \sum_{i=1}^{N} q_i, \tag{5.52}$$

$$M_z = \sum_{i=1}^{N} q_i z_i, \tag{5.53}$$

$$\Omega_z = \sum_{i=1}^{N} q_i z_i^2. \tag{5.54}$$

where N is the total number of particles. We note that for charge neutrality we will have $Q_t = 0$. We also define for each region

$$Q_l = \sum_{i=1}^{N_l} q_i, \tag{5.55}$$

$$M_{z,l} = \sum_{i=1}^{N_l} q_i z_i \tag{5.56}$$

$$\Omega_{z,l} = \sum_{i=1}^{N,l} q_i z_i^2. \tag{5.57}$$

where $l = 1, 2, 3$ for the regions I, II, III, respectively. So $Q_t = Q_1 + Q_2 + Q_3$ and $M_z = M_{z,1} + M_{z,2} + M_{z,3}$.

The indices i and j in Eq. (5.43) require some care. For each region the upper limit of the sums in U_{Ew} and U_p will be the number of particles N_l in that region at a particular simulation step. But the sums in U_Φ will be split in three contributions - one for each region, given by Eq. (5.40), (5.41), and (5.42) - with different upper limits for i and j.

5.3.1 Energy on region I

For this region of the system ($z < -h$), the contribution U_γ arises from the $k \to 0$ limit. For $\gamma = -1$ we have

$$U_{(-1)} = -\frac{2\pi}{L_d^2} Q_1 (M_{z,1} + Q_1 h). \tag{5.58}$$

The energy $U_{p'}$ due to surface polarizability can be written as

$$U_{p'} = \frac{\pi}{\epsilon L_d^2} \sum_{\boldsymbol{m'}} \frac{\gamma e^{-kh}}{k} \left(f_3(\boldsymbol{m})^2 + f_4(\boldsymbol{m})^2 \right), \tag{5.59}$$

where we use N_1 in the upper limit of the $f_i(\boldsymbol{m})$ functions.

The energy U_ϕ due to surface potentials is written after we sum the contributions from Eqs. 5.40, 5.41, and 5.42. Then we have

$$U_\phi = +\frac{\pi}{L_d^2}[Q_t M_{z,1} + Q_1(M_{z,1} - M_{z,2} - M_{z,3}) + Q_1 Q_t(2h + L/2) - Q_1 Q_2 h]. \tag{5.60}$$

5.3.2 Energy on region II

For this region of the system ($0 < z < L$) the contribution U_γ arises from the $k \to 0$ limit. For $\gamma = -1$ we have

$$U_{(-1)} = -\frac{2\pi}{L_d^2}\left[\frac{M_{z,2}^2}{L} - Q_2 M_{z,2}\right]. \tag{5.61}$$

The energy $U_{p'}$ due to surface polarizability can be written as

$$U_{p'} = \frac{\pi}{\epsilon L_d^2}\sum_{\boldsymbol{m'}} \frac{\gamma}{k(1-\gamma^2 e^{-2kL})}\{f_1(\boldsymbol{m})^2 + f_2(\boldsymbol{m})^2 + e^{-2kL}\left(f_1(\boldsymbol{m})^2 + f_2(\boldsymbol{m})^2\right) + 2\gamma e^{-2kL}\left(f_1(\boldsymbol{m}) f_3(\boldsymbol{m}) + f_2(\boldsymbol{m}) f_4(\boldsymbol{m})\right)\}, \tag{5.62}$$

where we use N_2 in the upper limit of the $f_i(\boldsymbol{m})$ functions. The energy U_ϕ due to surface potentials is written after we sum the contributions from Eqs. 5.40, 5.41, and 5.42. Then we have

$$U_\phi = +\frac{\pi}{L_d^2}[M_{z,2}(Q_3 - 2Q_2 - Q_1) - Q_2(M_{z,3} - M_{z,1}) + Q_2(Q_1 + Q_3)(h + L/2) + Q_2^2\frac{L}{2} + M_{z,2}^2\frac{2}{L}]. \tag{5.63}$$

5.3.3 Energy on region III

For this region of the system ($z > L + h$) the contribution U_γ arises from the $k \to 0$ limit. For $\gamma = -1$ we have

$$U_{(-1)} = +\frac{2\pi}{L_d^2} Q_3(M_{z,3} + Q_3(L + h)). \tag{5.64}$$

The energy $U_{p'}$ due to surface polarizability can be written as

$$U_{p'} = \frac{\pi}{\epsilon L_d^2}\sum_{\boldsymbol{m'}} \frac{\gamma e^{k(L+h)}}{k}\left(f_1(\boldsymbol{m})^2 + f_2(\boldsymbol{m})^2\right), \tag{5.65}$$

where we use N_3 in the upper limit of the $f_i(\boldsymbol{m})$ functions.

The energy U_ϕ due to surface potentials is written after we sum the contributions from Eqs. 5.40, 5.41, and 5.42. Then we have

$$U_\phi = -\frac{\pi}{L_d^2}[Q_t M_{z,3} + Q_3(M_{z,3} - M_{z,1} - M_{z,2}) \\ - Q_3 Q_t(h + L/2) - Q_3^2(h + 2L) - Q_1 Q_3 h]. \tag{5.66}$$

5.4 Monte Carlo simulations

In order to test this new method, we perform Monte Carlo simulations using the Metropolis algorithm [4] for a charged solution in the NVT ensemble (see Fig. 16). The simulations are similar to the ones made on Refs. [7] and [65]. The phase space is sampled using short and long displacement moves [9, 10]. The effective ionic radii are set to $r_c = 2$ Å. The Bjerrum length is defined as $q^2\beta/\epsilon_w$, where β is the inverse thermal energy and q is the proton charge. We set it to 7.2 Å, typical value for water at room temperature. The system relaxes to equilibrium in 5×10^5 Monte Carlo steps. The ionic density profiles are obtained using 5×10^4 uncorrelated samples.

We note that k depends on $\boldsymbol{m}$ and the f functions must be updated for each particle move. There is no need to recalculate all the functions, but only the contribution to each function that depends on the position of the particle that is being moved. This makes the energy update very efficient. Also, an essencial characteristic of the algorithm is that the components of the total energy are again decoupled both from each other and between different regions (with the exception of the terms U_ϕ that come from the surface potentials and which interact with all regions).

The vast majority of the calculations on each step can be performed on a parallel manner. If the code is written carefully with that intent, the automatic parallelizatoin procedures of the GNU and Intel compilers already detect this, resulting in a total computation 2 to 3 times faster. Also, we noticed that there is a symmetry between all k, which allowed us to rewrite the algorithm in a way that actually only calculates half the k terms (the other half is identical by symmetry).

Since the particles are moving between regions, additional care is required when recalculating the contributions of each function. This is because the majority of the contributions are affected only by the charges that exist in the region in which the calculation is being carried out, and the charges are free to move between regions.

In Fig. 17 there is the density profiles of cations and anions of metal plates in a dissolved 1:1 electrolyte at concentration 0.1 M, distance between the plates $L = 40$Å, $\gamma = -1$, $\lambda_B = 7.2$Å, and ionic radius to 2Å. We see an expected small attraction of charges to the neutral metal plates.

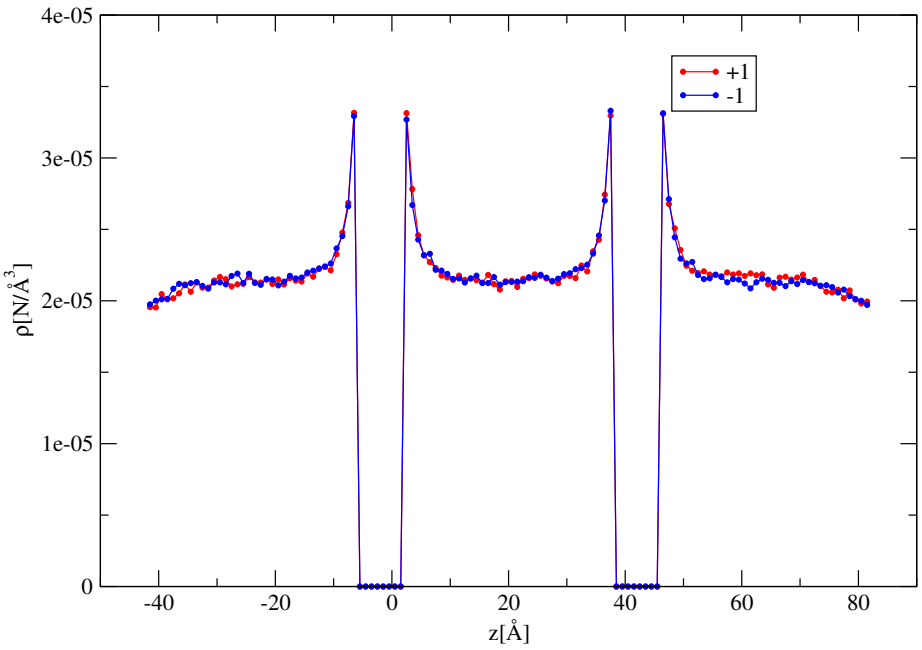

Figure 17: Density profiles of cations and anions in a dissolved 1:1 electrolyte at concentration 0.1 M, distance between the plates $L = 40$Å, $\gamma = -1$, $\lambda_B = 7.2$Å, ionic radius to 2Å.

In Fig. 18 there is the density profiles of cations and anions of metal plates in a dissolved 3:1 electrolyte at concentration 0.1 M, distance between the plates $L = 50$Å, $\gamma = -1$, $\lambda_B = 7.2$Å, and ionic radius to 2Å. We see an expected big attraction of the trivalent ions to the neutral metal plates.

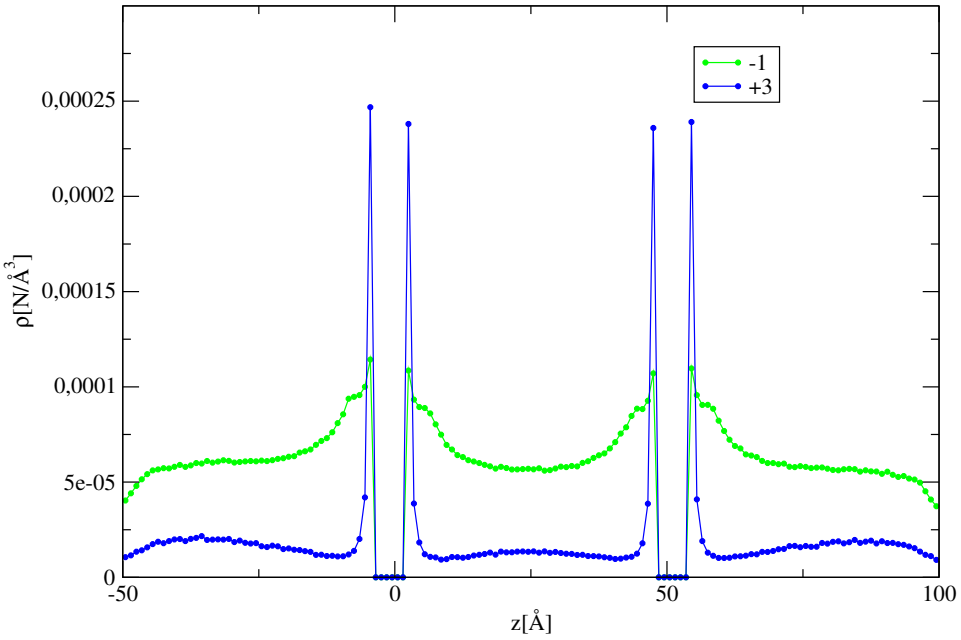

Figure 18: Density profiles of cations and anions of metal plates in a dissolved 3:1 electrolyte at concentration 0.1 M, distance between the plates $L = 50$Å, $\lambda_B = 7.2$Å, ionic radius to 2Å.

6 Conclusions

In this Dissertation we reviewed two algorithms to simulate confined charge fluids. The first one was a recently developed 3D Ewald summation technique for bulk systems [7]. This algorithm gains computational time by treating the charged walls as external linear potentials.

Then we reviewed another recent method for simulating Coulomb systems confined by general polarizable walls. It solves the Poisson Equation with the periodic eigenfunctions of the Laplace operator, resulting in a periodic Green function for the potential of the system. The energy can be split into contributions due to direct Coulomb interactions (which can be computed using already developed methods, like the one reviewed before), and due to polarization effects, which are written in a conventional form and don't recquire much computer power.

For example, in Fig. 19 there is characteristic central processing unit (CPU) times of this simulation method with a standard implementation of Lekner Summation which does not account for polarization [29], from which we can see that the Lekner Summation is at least an order of magnitude slower than this method for reasonably large system sizes, and even for systems with polarization and large N_c.

These advantages also apply for the new method developed here, which can be seen as an extension of those two to include the bulk. However, instead of one simulation box, now we have three. We showed that the energy can be split in the same manner. In this case there is again the Coulombic contribution, which is computed for each region separately. The polarization contribution is different for each region. There is an already known expression for the central region and we calculated the new expression for the outer regions. And then there is an extra contribution to account for the surface potentials of the induced charges, which is linear and cheap computationally. Again there is no need for a recalculation of all the energetic contribution at each step. Then we tested the method obtaining density profiles of monovalent and trivalent ions. The profiles in the central region were compared to already known results and the outer regions will be compared to a mean field theory that we are developing. Currently we are working to extend the application of the method by calculating the forces between the plates and by testing the

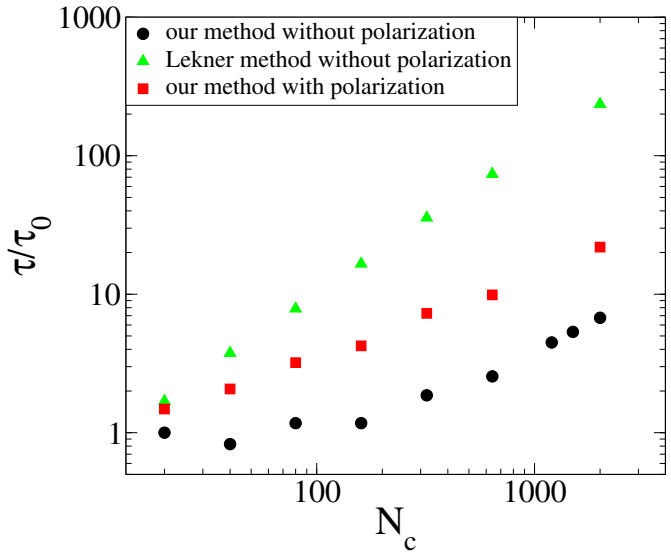

Figure 19: CPU time to perform 10^6 energy updates as a function of the number of particles in the system. The distance between the polarizable plates is $L = 10$Å, with $\gamma = 0.95$. The Bjerrum length was set to $\lambda_B = 14.5$Å, the superficial charge to $\sigma = -0.12\text{C/m}^2$ and ionic radius to 2Å. τ_0 is the CPU time to perform 10^6 energy updates.

same system with extra charge on the slabs.

Computationally, we will investigate further the implications of the decoupled nature of most of the calculations, such as the possibility of parallel methods [69] and accelerated simulations via cluster computing [70]. The parallel tempering [71] or replica exchange [72] approaches propose to accelerate Monte Carlo algorithms by simulating multiple copies of the system simultaneously in order to attempt additional interchanges beyond the single site trial moves. This technique has been compared with canonical Monte Carlo and molecular dynamics [73].

Another possibility is the particle–particle particle–mesh (PPPM) method algorithm [74], which uses the fast Fourier transform to develop further the Ewald method. Two of the more important mesh algorithms based on this idea are the particle mesh Ewald method [12] and the smooth particle mesh Ewald method [11]. We believe our methods could be made faster by adopting PPPM approaches [14, 15].

References

[1] O K Rice. On The Statistical Mechanics of Liquids. *J. Chem. Phys.*, 12:1–18, 1944.

[2] N Metropolis and S Ulam. The monte carlo method. *Journal of the American Statistical Association*, 44(247):335–341, 1949.

[3] N G Cooper, R Eckhardt, and N Shera. *From Cardinals to Chaos: Reflection on the Life and Legacy of Stanislaw Ulam.* Cambridge University Press, 1989.

[4] N Metropolis, A W Rosenbluth, M N Rosenbluth, A H Teller, and E Teller. Equation of State Calculations by Fast Computing Machines. *J. Chem. Phys.*, 21:1087–1092, 1953.

[5] D Landau and K Binder. *A Guide to Monte Carlo Simulations in Statistical Physics.* Cambridge University Press, 2005.

[6] W W Wood and F R Parker. Monte Carlo Equation of State of Molecules Interacting with the Lennard-Jones Potential. I. A Supercritical Isotherm at about Twice the Critical Temperature. *The Journal of Chemical Physics*, 27(3):720–733, 1957.

[7] A P dos Santos, M Girotto, and Y Levin. Simulations of Coulomb Systems with Slab Geometry Using an Efficient 3D Ewald Summation Method. *J. Chem. Phys.*, 144:144103–144109, 2016.

[8] P Ewald. Die Berechnung Optischer und Elektrostatischer Gitterpotentiale. *Ann. Phys.*, 369:253–287, 1921.

[9] Allen, M. P. and Tildesley, D. J. *Computer Simulation of Liquids: Second Edition.* Oxford: Oxford University Press, New York, United States of America, 2017.

[10] Frenkel D. and Smit, B. *Understanding Molecular Simulation.* Academic, San Diego, United States of America, 2002.

[11] U Essmann, L Perera, M L Berkowitz, T Darden, H Lee, and L G Pedersen. A Smooth Particle Mesh Ewald Method. *J. Chem. Phys.*, 103:8577–8593, 1995.

[12] T Darden, D York, and L Pedersen. Particle Mesh Ewald: An $N\dot{\log}(N)$ Method for Ewald Sums in Large Systems. *J. Chem. Phys.*, 98:10089–10092, 1993.

[13] J Kolafa and J W Perram. Cutoff Errors in the Ewald Summation Formulae for Point Charge Systems. *Mol. Simul.*, 9:351–368, 1992.

[14] M Deserno and C Holm. How to Mesh Up Ewald Sums. I. An Accurate Error Estimate for the Particle-Particle-Particle-Mesh Algorithm. *J. Chem. Phys.*, 109:7678–7693, 1998.

[15] M Deserno and C Holm. How to Mesh Up Ewald Sums. II. An Accurate Error Estimate for the Particle-Particle-Particle-Mesh Algorithm. *J. Chem. Phys.*, 109:7694–7701, 1998.

[16] Z Hu. Infinite Boundary Terms of Ewald Sums and Pairwise Interactions for Electrostatics in Bulk and at Interfaces. *J. Chem. Theory Comput.*, 10:5254–5264, 2014.

[17] M V Fedorov and A A Kornishev. Ionic Liquids at Electrified Interfaces. *Chem. Rev.*, 114:2978–3036, 2014.

[18] S Reed, O Lanning, and P Madden. Electrochemical Interface between an Ionic Liquid and a Model Metallic Electrode. *J. Chem. Phys.*, 126:084704, 2007.

[19] C Lian, K Liu, K L Van Aken, Y Gogotsi, D J Wesolowski, H L Liu, D E Jiang, and J Z Wu. Enhancing the Capacitive Performance of Electric Double-Layer Capacitors with Ionic Liquid Mixtures. *ACS Energy Lett.*, 1:21–26, 2016.

[20] M Dudka, S Kondrat, A Kornyshev, and G Oshanin. Phase Behavior and Structure of a Superionic Liquid in Nonpolarized Nanoconfinement. *J. Phys.: Condens. Matt.*, 28:466007, 2016.

[21] S Coles, M Mishin, S Perkin, M Fedorov, and V Ivanistsev. The Nanostructure of a Lithium Glyme Solvate Ionic Liquid at Electrified Interfaces. *Phys. Chem. Chem. Phys.*, 19:11004–11010, 2017.

[22] M Girotto, T Colla, A dos Santos, and Y Levin. Lattice Model of an Ionic Liquid at an Electrified Interface. *J. Phys. Chem. B*, 121:6408–6415, 2017.

[23] C Wong and M Muthukumar. Polymer Capture by Electro-Osmotic Flow of Oppositely Charged Nanopores. *J. Chem. Phys.*, 126:164903–164905, 2007.

[24] P Cazade, R Hartkamp, and B Coasne. Structure and Dynamics of an Electrolyte Confined in Charged Nanopores. *J. Phys. Chem. C*, 118:5061–5072, 2014.

[25] S Kondrat, N Georgi, M Fedorov, and A Kornyshev. A Superionic State in Nano-Porous Double-Layer Capacitors: Insights from Monte Carlo Simulations. *Phys. Chem. Chem. Phys.*, 13:11359–11366, 2013.

[26] A P dos Santos and Y Levin. Electrolytes between Dielectric Charged Surfaces: Simulations and Theory. *J. Chem. Phys.*, 142:194104, 2015.

[27] T Colla, M Girotto, A P dos Santos, and Y Levin. Charge Neutrality Breakdown in Confined Aqueous Electrolytes: Theory and Simulation. *J. Chem. Phys.*, 145:094704, 2016.

[28] Z Luo, Y Xing, Y Ling, A Kleinhammes, and Y Wu. Electroneutrality Breakdown and Specific Ion Effects in Nanoconfined Aqueous Electrolytes Observed by NMR. *Nat. Commun.*, 6:6358–6365, 2015.

[29] J Lekner. Summation of Coulomb Fields in Computer-Simulated Disordered Systems. *Physica A*, 176:485–498, 1991.

[30] A H Widmann and D B Adolf. A Comparison of Ewald Summation Techniques for Planar Surfaces. *Comput. Phys. Commun.*, 107:167–186, 1997.

[31] Y Levin. Electrostatic Correlations: from Plasma to Biology. *Rep. Prog. Phys.*, 65:1577, 2002.

[32] Alberto Martin-Molina, Jose Guadalupe Ibarra-Armenta, Enrique Gonzalez-Tovar, Roque Hidalgo-Alvarez, and Manuel Quesada-Perez. Monte Carlo Simulations of The Electrical Double Layer Forces in The Presence of Divalent Electrolyte Solutions: Effect of The Ion Size. *Soft Matter*, 7:1441–1449, 2011.

[33] A Grosberg, T Nguyen, and B Shklovskii. Colloquium: The Physics of Charge Inversion in Chemical and Biological Systems. *Rev. Mod. Phys.*, 329:329–345, 2002.

[34] Z Wang and J Wu. Ion Association at Discretly-Charged Dielectric Interfaces: Giant Charge Inversion. *J. Chem. Phys.*, 147:024703, 2017.

[35] L Šamaj and E Trizac. Counterions at Highly Charged Interfaces: From One Plate to Like-Charge Attraction. *Phys. Rev. Lett.*, 106:078301, 2011.

[36] M Hatlo and L Lue. Electrostatic Interactions of Charged Bodies from The Weak-to-The-Strong-Coupling Regime. *Euro. Phys. Lett.*, 89:25002, 2010.

[37] R Netz and H Orland. Beyond Poisson-Boltzmann: Fluctuation Effects and Correlation Functions. *The Euro. Phys. Journ. E*, 1:203–214, 2000.

[38] Y Levin. When Do Like Charges Attrack? *Physica A*, 265:432–439, 1999.

[39] I C Yeh and M L Berkowitz. Ewald Summation for Systems with Slab Geometry. *J. Chem. Phys.*, 111:3155–3162, 1999.

[40] M Kawata and M Mikami. Rapid Calculation of Two-Dimensional Ewald Summation. *Chem. Phys. Lett.*, 340:157–164, 2001.

[41] A Arnold, J de Joannis, and C Holm. Electrostatics in Periodic Slab Geometries. I. *J. Chem. Phys.*, 117:2496–2502, 2002.

[42] A Arnold, J de Joannis, and C Holm. Electrostatics in Periodic Slab Geometries. II . *J. Chem. Phys.*, 117:2503–2512, 2002.

[43] S Yi, C Pan, and Z Hu. Note: A Pairwise Form of The Ewald Sum for Non-Neutral Systems. *J. Chem. Phys.*, 147:126101, 2017.

[44] J I Siepmann and M Sprik. Influence of Surface Topology and Electrostatic Potential on Water/Electrode Systems. *J. Chem. Phys.*, 102:511–524, 1995.

[45] J Zwanikken and M de la Cruz. Tunable Soft Structure in Charged Fluids Confined by Dielectric Interfaces. *Proc. Natl. Acad. Sci. U.S.A.*, 110:5301–5308, 2013.

[46] D T Limmer, C Merlet, M Sallane, D Chandler, P A Madden, R van Roij, and B Rotenberg. Charge Fluctuations in Nanoscale Capacitors. *Phys. Rev. Lett.*, 111:106102–106106, 2013.

[47] C Merlet, D T Limmer, M Salanne, R van Roij, P A Madden, D Chandler, and B Rotenberg. The Electric Double Layer Has a Life of Its Own. *J. Phys. Chem. C*, 118:18291–18298, 2014.

[48] A Arnold, K Breitsprecher, F Fahrenberger, S Kesselheim, O Lenz, and C Holm. Efficient Algorithms for Electrostatic Interactions Including Dielectric Contrasts. *Entropy*, 15:4569–4588, 2013.

[49] S Tyagi, A Arnold, and C Holm. ICMMM2D: An Accurate Method to Include Planar Dielectric Interfaces via Image Charge Summation. *J. Chem. Phys.*, 127:154723, 2007.

[50] S Tyagi, A Arnold, and C Holm. Electrostatic Layer Correction with Image Charges: A Linear Scaling Method to Treat Slab 2D+h Systems with Dielectric Interfaces. *J. Chem. Phys.*, 129:204102, 2008.

[51] Z Gan, H Wu, K Barros, Z Xu, and E Luijten. Comparison of Efficient Techniques for The Simulation of Dielectric Objects in Electrolytes. *J. Comp. Phys.*, 291:317–333, 2015.

[52] S Tyagi, M Süzen, M Sega, M Barbosa, S Kantarovitch, and C Holm. An Iterative, Fast, Linear-Scaling Method for Computing Induced Charges on Arbitrary Dielectric Boundaries. *J. Chem. Phys.*, 132:154112, 2010.

[53] D Boda, D Gillespie, W Nonner, D Henderson, and B Eisenberg. Computing Induced Charges in Inhomogeneous Dielectric Media: Application in a Monte Carlo Simulation of Complex Ionic Systems. *Phys. Rev. E*, 69:046702, 2004.

[54] M Armand, F Endres, D R MacFarlane, H Ohno, and B Scrosati. Ionic-Liquid Materials for The Electrochemical Challenges of the Future. *Nat. Mat.*, 8:621–629, 2009.

[55] X Kong, D Lu, Z Liu, and J Wu. Molecular Dynamics for the Charging Behavior of Nanostructured Electric Double Layer Capacitors containing Room Temperature Ionic Liquids. *Nano Research*, 8:931–940, 2015.

[56] S. Kondrat and A. Kornyshev. Superionic State in Double-Layer Capacitors with Nanoporous Electrodes. *J. Phys.: Condens. Matter*, 23(2):022201, 2011.

[57] P Simon and Y Gogotsi. Materials For Electrochemical Capacitors. *Nat. Mat.*, 7:845–854, 2008.

[58] M Chen, S Li, and G Feng. The Influence of Anion Shape on the Electrical Double Layer Microstructure and Capacitance of Ionic Liquids-Based Supercapacitors by Molecular Simulations. *Molecules*, 22:241–242, 2017.

[59] J Wishart. Energy Applications of Ionic Liquids. *Energy Environ. Sci.*, 2:956–961, 2009.

[60] F Zhou, Y Liang, and W Liu. Ionic Liquid Lubricants: Designed Chemistry for Engineering Applications. *Chem. Soc. Rev.*, 38:2590–2599, 2009.

[61] S Ito, S M Zakeeruddin, P Comte, P Liska, D Kuang, and M Grätzel. Bifacial Dye-Sensitized Solar Cells Based on an Ionic Liquid Electrolyte. *Nat. Photonics*, 2:693–698, 2008.

[62] Q Li, Q Tang, B He, and P Yang. Full Ionic-Liquid Gel Electrolytes: Enhanced Photovoltaic Performances in Dye-Sensitized Solar Cells. *J. Power Sources*, 264:83–91, 2014.

[63] M Girotto, R M Malossi, A P dos Santos, and Y Levin. Lattice model of ionic liquid confined by metal electrodes. *The Journal of Chemical Physics*, 148(19):193829, 2018.

[64] M Girotto, A P dos Santos, and Y Levin. Simulations of Ionic Liquids Confined by Metal Electrodes Using Periodic Green Functions. *J. Chem. Phys.*, 147:074109, 2017.

[65] A P dos Santos, M Girotto, and Y Levin. Simulations of Coulomb Systems Confined by Polarizable Surfaces Using Periodic Green Functions. *J. Chem. Phys.*, 147:184105, 2017.

[66] M Girotto. *Simulations of confined charged systems*. PhD thesis, Federal University of Rio Grande do Sul, 2018.

[67] Russel, W. B., Saville, D. A. and Schowalter, W. R. *Colloidal Dispersions*. Cambridge University Press, New York, United States of America, 1989.

[68] A P dos Santos, M Girotto, and Y Levin. Simulations of Polyelectrolyte Adsorption to a Dielectric Like-Charged Surface. *J. Phys. Chem. B*, 120:10387–10393, 2016.

[69] K Esselink, L D J C Loyens, and B Smit. Parallel monte carlo simulations. *Phys. Rev. E*, 51:1560–1568, 1995.

[70] R Ren and G Orkoulas. Parallel markov chain monte carlo simulations. *The Journal of Chemical Physics*, 126(21):211102, 2007.

[71] K Hukushima and K Nemoto. Exchange monte carlo method and application to spin glass simulations. *Journal of the Physical Society of Japan*, 65(6):1604–1608, 1996.

[72] R H Swendsen and J Wang. Replica monte carlo simulation of spin-glasses. *Phys. Rev. Lett.*, 57:2607–2609, 1986.

[73] U Hansmann. Parallel tempering algorithm for conformational studies of biological molecules. *Chemical Physics Letters*, 281(1):140 – 150, 1997.

[74] J W Eastwood, R W Hockney, and D N Lawrence. P3m3dp-the three-dimensional periodic particle-particle/particle-mesh program. *Computer Physics Communications*, 35:C–618 – C–619, 1984.

[75] Y Levin. Electrostatics of Ions Inside The Nanopores and Trans-Membrane Channels. *Europhys. Lett.*, 76:163, 2006.

[76] K Kiyohara and K Asaka. Monte Carlo Simulation of Electrolytes in The Constant Voltage Ensemble. *J. Chem. Phys.*, 126:214704–214717, 2007.

[77] M N Kobrak. The Relationship between Solvent Polarity and Molar Volume in Room-Temperature Ionic Liquids. *Green Chem.*, 10:80–86, 2008.

[78] M.-M Huang, Y Jiang, P Sasisanker, G W Driver, and H Weingartner. Static Relative Dielectric Permittivities of Ionic Liquids at 25° C. *J. Chem. Eng. Data*, 56:1494–1499, 2011.

[79] A A Kornyshev. Double-layer in ionic liquids: Paradigm change? *J. Phys. Chem. B*, 111:5545–5557, 2007.

[80] A Panagiotopoulos. Large Lattice Discretization Effects on the Phase Coexistence of Ionic Liquids. *Phys. Rev. Lett.*, 83:2981–2984, 1999.